UNIVERSITÄTSKLINIKUM HAMBURG-EPPENDORF

Institut für Neuroanatomie

Zentrum für Experimentelle Medizin

Professor Dr. Gabriele M. Rune

Sexually differentiated microglia and CA1 hippocampal synaptic connectivity

Dissertation

zur Erlangung des Grades eines Doktors der Medizin
an der Medizinischen Fakultät der Universität Hamburg.

vorgelegt von:

Tim Michael Prengel
aus Hofgeismar

Hamburg 2024

Angenommen von der
Medizinischen Fakultät der Universität Hamburg am: 18.11.2024

Veröffentlicht mit Genehmigung der
Medizinischen Fakultät der Universität Hamburg.

Prüfungsausschuss, der/die Vorsitzende: Prof. Dr. Matthias Kneussel

Prüfungsausschuss, zweite/r Gutachter/in: Prof. Dr. Gabriele Rune

Inhaltsverzeichnis

Received: 9 January 2023 | Revised: 14 March 2023 | Accepted: 31 March 2023

DOI: 10.1111/jne.13276

ORIGINAL ARTICLE

Journal of Neuroendocrinology WILEY

Sexually differentiated microglia and CA1 hippocampal synaptic connectivity

Tim M. Prengel[1] | Bianka Brunne[1] | Moataz Habiballa[1] | Gabriele M. Rune[2]

[1]Institute of Neuroanatomy, University Medical Center Hamburg Eppendorf, Hamburg, Germany

[2]Institute of Cell Biology and Neurobiology, Charité Universitätsmedizin Berlin, Berlin, Germany

Correspondence
Gabriele M. Rune, Charité Universitätsmedizin Berlin, Institut für Zell- und Neurobiologie, Charitéplatz 1, 10117 Berlin, Germany. Email: gabriele.rune@charite.de

Funding information
Deutsche Forschungsgemeinschaft, Grant/Award Number: DFG 436/7-1

Abstract

Microglia have been shown to sculpt postnatal circuitry from birth up to adulthood due to their role in both synapse formation, synaptic pruning, and the elimination of weak, redundant synapses. Microglia are differentiated in a sex-dependent manner. In this study, we tested whether sexual differentiation of microglia results in sexdependent postnatal reorganization of CA1 synaptic connectivity in the hippocampus. The stereological counting of synapses in mice using electron microscopy showed a continuous rise in synapse density until the fourth week, followed by a plateau phase and loss of synapses from the eighth week onwards, with no difference between sexes. This course of alteration in synapse numbers did not differ between sexes. However, selectively, on postnatal day (P) 14 the density of synapses was significantly higher in the female than in the male hippocampus. Higher synapse density in females was paralleled by higher activity of microglia, as indicated by morphological changes, CD68 expression, and proximity of microglia to synaptic sites. In Thy1-GFP mice, consistent with increased synapse numbers, bouton density was also clearly increased in females at P14. At this time point, CD47 expression, the “don't eat me” signal of neurons, was similar in males and females. The decrease in bouton density thereafter in conjunction with increased synapse numbers argues for a role of microglia in the formation of multispine boutons (MSB). Our data in females at P14 support the regulatory role of microglia in synapse density. Sexual differentiation of microglia, however, does not substantially affect long-term synaptic reorganization in the hippocampus.

KEYWORDS

electron microscopy, hippocampus, microglia, sex-specificity, synaptic pruning

1 | INTRODUCTION

Remodeling of neuronal circuitry during postnatal development from birth to adulthood includes synaptogenesis on the one hand, but also the elimination, pruning of weak, redundant synapses on the other hand. During early postnatal brain development, synapse formation exceeds that of elimination, which results in an excess of excitatory synapses. Excess synapses are subsequently eliminated or pruned in the adolescent brain, thus leading to fewer synapses in the adult.[1] This type of synaptic remodeling after birth has been described for different species and brain areas, including the hippocampus.[2–4] Proper refinement of neural circuitry after birth, in turn, is required for normal cerebral development and delayed synaptic pruning frequently underlies intellectual disabilities in adults.[5–7]

It has been shown that microglia substantially contribute to remodeling of neuronal circuitry (for review see[8]). In this context, it is of note, that microglia have bidirectional roles: on the one hand in establishing synaptic connenctions,[2,9] and on the other hand, in synaptic pruning, since supernumerary synapses have been demonstrated to be engulfed by microglia.[10–12]

Microglia are sexually differentiated, either by sex chromosome, sex hormones or indirectly by microenvironmental changes, and they are involved in sex-specific processes of differentiation in the brain.[13–18] In several studies, these differences were assumed to be mainly due to sex-specific levels of sex hormones during the critical perinatal period,[19–21] and microglia have also been shown to express estrogen receptors in a sex-dependent manner.[22] Regarding synaptic pruning, robust sex differences have been found in the expression of several phagocytic pathway genes,[19] and in another study the number of phagocytic microglia in females was reduced to male typical levels in response to estradiol treatment.[23] With respect to synaptogenesis, the effect of estradiol on inducing spine formation depends on the presence and function of microglia.[9] Altogether, these studies support responsiveness of microglia to sex steroids[20,24] and raise the question as to whether varying levels of sex hormones during adolescence and puberty up to adulthood may result in differences between sexes.

Weinhard and coworkers[21] studied sex differences in microglia volume and phagocytic capacity across postnatal development and found, after 1 week, more active microglia in females, and after four postnatal weeks, more active microglia in males. Increased microglial activity was paralleled by increased spine and bouton density in female Thy1-GFP mice at 1 week, but unfortunately synaptic connectivity was not studied after 4 weeks. These findings prompted us to re-evaluate synaptic connectivity after one and two weeks after birth and furthermore, to study synapse density at 3, 4, 8 and 12 postnatal weeks in the CA1 hippocampal region, as synaptic refinement continues until adulthood.[4] Finally, the density of dendritic spines and boutons, or the expression of synaptic proteins, which were used by Weinhard et al.[21] as parameters of synaptic connectivity, are not necessarily indicative of synapse numbers. Quantitative ultrastructural data on hippocampal synapse densities, however, in the course of postnatal synaptic synaptogenesis and pruning are so far missing.

Except for the second postnatal week, there was no difference in the dynamics of synapse development and in synapse densities in males and females. Only on P14 was stronger activity of microglia in females paralleled by higher synapse density. Upregulated activity of microglia between P7 and P14 in females remains to be

J Neuroendocrinol.
2023;35:e13276. https://doi.org/10.1111/jne.13276

clarified, but may underlie increased synapse and bouton numbers in females compared to males. In contrast, microglia's sexual differentiation is unlikely to influence synapse numbers in a sex specific manner during later postnatal development.

2 | MATERIALS AND METHODS

2.1 | Animals

All mouse strains were maintained on a C57Bl6/J background. Backcrossing was performed at least every third generation. The mice were housed under standard conditions, with food and water provided ad libitum. Experiments were conducted in accordance with the German and European Union laws on protection of experimental animals following approval by the local authorities of the City of Hamburg (Committee for Lebensmittelsicherheit und Veterinärwesen, Authority of Soziales, Familie, Gesundheit und Verbraucherschutz Hamburg, Germany).

A total of 36 C57BL/6J mice (3–4 animals per sex at P14, P21, P28, P56 and P84) were used for electron microscopy. Each group consisted of mice from two litters. In the P14 group, all males and one female were littermates, the other three females were taken from a different litter. The P21 group was entirely taken from one litter. A total of 18 Thy1eGFP heterozygous mice[25] were used for immunohistochemistry (three animals per sex at P7, P14, P21).

The P14 mice were taken from three different litters, with two males and two females being littermates and one male and one female from two different litters. The P21 mice were taken from two litters with all males and one female being littermates and two females from a different litter. Six wild-type littermates were used for western blot analysis (three animals per sex at P14). Six C57BL/6J mice (three animals per sex at P14) were used for RNA in situ hybridization with RNA Scope. All animals were first anesthetized using 80% CO_2/20% O_2 inhalation and sacrificed with 100% CO_2 inhalation.

2.2 | Electron microscopy

Animals for electron microscopy were transcardially perfused with 2.5% glutaraldehyde in phosphate buffered saline (PBS). The brains were removed and postfixed overnight at 4C. The hippocampi were dissected out of the brains and divided into dorsal and ventral parts. Following fixation in 2.5% glutaraldehyde overnight, the samples were postfixed in 1% OsO_4 for 2 h. Subsequently, the samples were dehydrated in graded ethanol starting with 35% and progressing to 100% followed by propylene oxide. The dehydrated samples were then embedded in Epon 820 (Serva). The blocks were trimmed and cut in thin sections on a Reichert-Jung OmU3 ultramicrotome. The ultrathin sections were contrasted with uranyl acetate, followed by lead citrate (for more detail see[26,27]).

Spine synapse density was calculated using unbiased stereological methods. Consecutive serial ultrathin sections from the CA1 striatum were cut and placed on formvar-coated single grids. Digitized images were taken at a magnification of 2600x (CM100 electron microscope, Philips, Germany). The dissector technique was used to obtain a comparable measure of synaptic numbers, unbiased for possible changes in synaptic size.[28] To calculate the spine synapse density on pyramidal cell dendrites, a reference grid was superimposed on the electron microscopic prints. Only those spine synapses were counted that were on the reference section but not on the consecutive section. The dissector volume (6.4 μm^3) was calculated by multiplying the unit area of the reference grid (8 8 μm) by the distance (0.1 μm) between the upper faces of the reference and the consecutive section (see also[29–32]).

For each animal, at least 15 neuropil volumes, consisting of a reference and a consecutive section, were analyzed. The observer was blinded to the experimental group.

2.3 | Immunofluorescence

Thy1-eGFP-positive mice of 2 and 3 weeks of age were transcardially perfused with PBS. Brains were removed and postfixed in 4% paraformaldehyde (PFA) in PBS over two nights, then washed three times in PBS and embedded in 4.5% agarose. One week old newborns were rapidly decapitated and after brain removal, treated in the same way as animals of 2 and 3 weeks of age.

After embedding, brains were coronally cut on a Leica vibratome in 50 μm thin consecutive slices and gathered in a 24-well plate. Then, slices were blocked with 10% horse-serum and 0.5% triton and primarily stained with P2Y12 (AnaSpec 55043A, rabbit, 1:500) and Iba1 (Synaptic Systems 234004, guinea pig, 1:600) or CD68 (Bio-Rad MC1957, rat, 1:100) antibodies for microglia and brain lipid-binding protein (BLBP: Merck-Millipore ABN14, rabbit, 1:500) and glial fibrillary acidic protein (GFAP: Dako Z033401-2, rabbit, 1:1000) antibodies for astrocytes, incubating for three nights at 4C. In addition to Iba1, we also used P2Y12 as a marker of microglia, since this receptor has been found expressed exclusively on microglia, where it is necessary for physiological and pathological microglial actions, such as monitoring neuronal functions and microglial neuroprotection.[33,34]

After incubation, slices were washed and secondary antibodies (GFP with Alexa 488, Thermofisher A21311, 1:1000; Anti-GP AF647 Invitrogen A21450, 1:500; anti-rabbit AF568, Abcam Ab175470, 1:500; anti-rat AF647, Thermofisher A21247, 1:500) were applied depending on primary staining and slices were incubated for another night. Finally, nuclei were stained for 30 min with 4^0, 6-diamidino-2-phenylindole (DAPI: Sigma-Aldrich, 1:5000) and five specimens each were mounted on an object slide with mowiol 4-88. During the whole process of secondary staining the specimens were kept in the dark.

Antibody specificity in immunohistochemistry was tested by omitting the primary antibody and by double-labeling experiments. For microglia we used Iba1 and P2Y12 and for astrocytes GFAP and BLBP. In both cases we found a complete overlap. Complete overlap was also found by using CD68 and P2Y12.

Images were obtained with a ZEISS AxioObserver with integrated Apotome 2 and Plan-APO 40/1.4/Oil Objective. The Apotome.2 system is a structured illumination system and provides image resolution that is similar to confocal imaging. This was already shown for the previous Apotome system.[35,36] Advantages include the fact that no cost-intensive laser is required and the lack of pixel wise scanning allows for quicker imaging.

For each image a region of interest in the CA1 field was located, and three individual pyramidal neurons with visible dendritic protrusions and up to six axons with visible synaptic boutons per animal in the stratum radiatum were chosen for examination. Since only a fraction of hippocampal neurons in the mouse hippocampus expresses eGFP,[37] the event of an eGFP positive axon interacting with an eGFP positive dendrite is very rare and axons and spines had to be evaluated separately. Z-stacks with at least 40 0.27 μm were recorded and deconvoluted using standard deconvolution parameters of ZEISS ZEN pro (version 3.0). Data was analyzed with Oxford Instruments Imaris (version 9.6.0) by a blinded investigator. For each z-stack a single dendrite of first order in distance between seven to 70 μm to the stratum pyramidalis was three-dimensionally reconstructed with an individually adjusted contrast threshold. Microglial spine contacts were assessed by measuring P2Y12 fluorescence intensity within spine heads reconstructed using the eGFP fluorescence signal. The analysis is based on fluorescence overlap between neighboring fluorescent structures, which has been extensively used in the analysis of morphogenesis of synaptic components.[38] In order to determine complete contacts with a low rate of false positive contacts, only spine heads with a P2Y12 intensity greater than 100 were considered positive for encapsulation and positive spines were verified for complete encapsulation by a blinded investigator. Average length of reconstructed dendrites was 64 μm and average dendrite diameter was 0.61 μm.

An identical approach was used to determine the contacts of spines by astrocytes, but because of an overall lower signal intensity in BLBP staining, spine heads displaying a BLBP intensity greater than 50 were considered positive.

Spine analysis were performed with the Imaris Classify Spines Xtension.[39] Spines were categorized as stubby spines (length <1 μm), mushroom spines (maximum length >3 μm and maximum head width at least two times greater than mean neck width), long thin spines (head width equals neck width) and filopodia (every spine not categorized as one of the above and with head width ≤ neck width). Axonal bouton density was determined by measuring the signal intensity of each axonal shaft, which were normalized across all datasets. Boutons were detected using the spot detection tool from Imaris with individual thresholding and were counted as positive when signal intensity of the bouton exceeded signal intensity of the axonal shaft by 40%.[21]

Microglia were reconstructed in Imaris based on P2Y12 immunohistochemistry. Reconstruction was performed in image volumes with a width and length of 80 μm and a depth of 10 μm, each located in the stratum radiatum of CA1. Surface to volume ratio (SVR) was calculated as a morphological parameter, which indirectly reflects the state of microglia activation (short thick processes lead to small surface to volume ratios, while long thin processes would lead to higher surface to volume ratios). SVR was calculated based on total surface of all reconstructed microglia parts within the image volume divided by the total volume of all reconstructed microglia parts within the same image volume.

TABLE 1 Raw data of glyceraldehyde-3-phosphate dehydrogenase (GAPDH) expression.

Age/sex	GAPDH rel. to 1
P14 male	1 (normalized)
P14 male	1.06
P14 male	0.98
P14 female	1.13
P14 female	1.33
P14 female	0.99

Note: GAPDH expression was homogenous with 83% less than one standard deviation from the mean and overall within two SD (mean = 1.08; SD = 0.13).

TABLE 2 Contingency table of microglia spine contacts.

Age/sex	Spines	Contacts	Total
P14 female	387	52 (12%, p = .0001)	439
Expected		31 (7%)	
Std. residues		4.79188	
P14 male	452	14 (3%, p = .0003)	466
Expected		33 (7%)	
Std. residues	3.59725	3.59725	
P21 female	609	42 (6%, n.s.)	651
Expected		46 (7%)	
Std. residues	0.31828	0.31828	
P21 male	636	42 (6%, n.s.)	678

2.4 | RNA scope

To evaluate microglia colonization at P14, a RNA, in situ hybridization was performed using the RNAscope technique[40] using the RNAscope kit (ACD biotechne). A target probe specific to P2Y12 mRNA (ACD biotechne 317601-C2) was used in cryo slices of three animals of each sex. After the hybridization process, images of both left and right hippocampi were taken with a 25/air objective and stitched together in Imaris. Then, rectangular planes with an average size of 75480 μm^2 from the CA1 field were analyzed for aggregations of P2Y12 RNA in colocalization with DAPI to quantify microglial nuclei.

2.5 | Western blot

WT-littermates of the Thy1-eGFP animals were used for protein anal-

Expected		48 (7%)	
Std. residues	0.64791	0.64791	
Total	2075	159	2234

ysis by western blot. The hippocampi were removed from the brain and frozen in liquid nitrogen. After thawing at 4C, the hippocampi were manually homogenized in radioimmunoprecipitation assay (RIPA) buffer and a mixture of proteinase (Roche cOmplete Tablets 1:25) and phosphatase inhibitors (Roche PhosSTOP 1:10). The samples were centrifuged at 13,000 rpm for 20 min at 4C, and the supernatants were frozen until further use. Then, 10 µg of each sample were run on a 10% SDS–PAGE and blotted on nitrocellulose membranes. Unspecific binding of antibodies was prevented by treatment of the membrane with 5% nonfat milk powder solution (in TBS plus 0.3% Tween). The incubation with the primary antibody was carried out in blocking solution for 12 h at 4C with CD47 antibody by RD Systems (goat 1:1000), and glyceraldehyde 3-phosphate dehydrogenase (GAPDH) was used as internal standard (Life Technology, mouse, 1:200). For secondary staining, HRP conjugated mouse-anti-goat (Thermofisher 1:200) and goat-anti-mouse (Thermofisher, 1:200) antibodies were used. Immunodetection was accomplished using the Immobilon western chemiluminescent HRP substrate (Merck Millipore), and the chemiluminescent signal was detected by the FUSIONSL4 advanced imaging system (Vilber) and quantified by densitometry

Note: To assess if the differences in microglia morphology affect the occurrence of microglia spine contacts, 2234 spines were categorized for the values contacted or not-contacted and, as a second variable, also categorized into four groups (P14 female, P14 male, P21 female, P21 male). Data was then applied to a contingency table. The largest deviation of observed from expected occurrence for contact frequency was found between the sexes at P14, with a four-fold higher rate in observed female spines compared to observed male spines. Pearson's chi-square test showed significance with no expected cell frequencies below five ($\chi^2(3) = 29.06$; $p = .0001$; Cramer's $V = 0.114$). Post hoc tests revealed high significance for the dependency of sex and spine-contacts at P14, with spines being twice as often frequented by microglia when they were female and only half as often frequented when they were male (P14 female: $p = .0001$; Cramer's $V = 0.1$; P14 male: $p = .0003$; Cramer's $V = 0.09$). Female P14 (12%) $p = .0001$; Male p14 (3%) $p = .0003$; Female P21 (6%) n.s.; Male p21 (6%) n.s.

TABLE 3 Contingency table of astrocyte spine contacts.

Age/sex	Spines	Contacts	Total
P14 female	530	7 (1.3%, n.s.)	537
Expected		11.5 (2.1%)	
Std. residues		1.3	
P14 male	354	6 (1.7%, n.s.)	360
Expected		7.7 (2.1%)	
Std. residues	0.1	0.6	
P21 female	333	5 (1.5%, n.s.)	338
Expected		7.2 (2.1%)	
Std. residues	0.1	0.8	
P21 male	429	18 (4%, p = .015)	447
Expected		9.6 (2.1%)	
Std. residues	0.4	2.7	
Total	1646	36	1682

Note: Astrocyte spine interactions were assessed in a similar approach to the assessment of microglia spine interactions and 1682 spines were categorized for the values contacted or not-contacted and, as a second variable, also categorized into four groups (P14 female, P14 male, P21 female, P21 male). Spines showed dependency for a higher contact frequency in males at P21 (Pearson's chi-square test $\chi^2(3) = 10.481$; $p = .015$; Cramer's $V = 0.08$). Female p14 (1.3%) n.s.; Male p14 (1.7%) n.s.; Female p21 (2.1%) n.s.; Male p21 (4%) $p = .015$.

TABLE 4 Statistical analysis

Figure	Data structure	Type of test	Sample size	Statistical data
1B	Not normally distributed	Nonlinear regression with centered variables	WT mice, n = 36	F(3) = 9.651; adjusted R^2= 0.475; p = .0001; SC Age = 3.971; p = .0001; SC Age =3.822; p = .0001; power: 0.996
1D				
P14	Normally distributed	Unpaired t-test (two-tailed) with bootstrapping	WT mice P14, n = 4	t = 3.153; df = 6; mean difference = 2.38; 95% CI (0.83; 3.6); p = .02; Cohen's d = 2.229
P21	Normally distributed	Unpaired t-test (two-tailed) with bootstrapping	WT mice P21, n = 4	t = 0.917; df = 6; mean difference = 0.77; 95% CI (0.65; 2.4); p = .39; Cohen's d = 0.65
P28	Normally distributed	Unpaired t-test (two-tailed) with bootstrapping	WT mice P28, n = 3	t = 0.52; df = 4; mean difference = 0.69; 95% CI (1.26; 3.2); p = .63; Cohen's d = 0.42
P56	Not normally distributed	Unpaired t-test (two-tailed) with bootstrapping	WT mice P56, n = 3	t = 0.957; df = 4; mean difference = 1.5; 95% CI (0.55; 4.63); p = .39; Cohen's d = 0.78
P84	Normally distributed	Unpaired t-test (two-tailed) with bootstrapping	WT mice P84, n = 4	t =0.279; df = 6; mean difference =0.46; 95% CI (3.56; 2.08); p = .78; Cohen's d = 0.19
2D	Normally distributed	One way ANOVA with Bonferroni post hoc testing	Thy1-eGFP mice, n = 3, two ROI per animal with 4 exclusions because of insufficient staining	F = 4.99; p = .002; η^2= 0.49; P7–P21 mean difference=0.57; 95% CI (1.0; 0.14); SE = 0.17; p = .008; P14 female–male mean difference =0.93; 95% CI (1.8; 0.05); SE = 0.27; p = .03
2E	Normally distributed	One way ANOVA with planned contrast	Thy1-eGFP mice, n = 3, one ROI per animal	F = 23.6; η^2= 0.115; mean difference 152.98; SE = 31.495; 95% CI (65.53; 240.42); p = .008
3D	Normally distributed	Unpaired t-test (two-tailed)	WT mice P14, n = 3	P14: t = 0.053; df = 10; mean difference = 0.066; 95% CI (2.7; 2.83); SE = 1.24; p = .96
4D	Categorial	Pearson's chi-square test with post hoc analysis	n = 2234, spines were categorized for microglia contacts and sex/age (spines were reconstructed from 12 Thy1-eGFP mice, 3 cells per mouse).	χ^2(3) = 29.06; p = .0001; Cramer's V = 0.114; power: 0.997 P14 female: p = .0001; Cramer's V = 0.1; P14 male: p = .0003; Cramer's V = 0.09
4F	Categorial	Pearson's chi-square test	n = 1682, spines were categorized for astrocyte contacts and sex/age (spines were reconstructed from 12 Thy1-eGFP mice, 3 cells per mouse).	χ^2(3) =10.481; p = .015; Cramer's V = 0.08; power: 0.79
5A	Normally distributed	Unpaired t-test (two-tailed)	Thy1-eGFP mice, n = 3, maximum 6 cells per animal	P14: t = 2179; df = 33; mean difference = 5.6; 95% CI (0.37; 10.84); SE = 2.57; p = .03
5B	Normally distributed	Unpaired t-test (two-tailed)	Thy1-eGFP mice, n = 3, three cells per animal	P14: t =0.44; df = 16; mean difference =0.63; 95% CI (3.67; 2.41); SE = 1.55; p = .66 P21: t =1.04; df = 16; mean difference =1.49; 95% CI (4.53; 1.55); SE = 1.55; p = .31
6	Normally distributed	Unpaired t-test (two-tailed)	WT mice P14 n = 3	t =1292; df = 4; mean difference =0.11; 95% CI (0.34; 0.12); SE = 0.08; p = .26

Note: p-values were controlled for a false discovery rate of Q = 0.1 with the Benjamini-Hochberg procedure.
Abbreviations: ANOVA, analysis of variance; CI, confidence interval; ROI, region of interest.

using the software ImageJ (NCBI). We used GAPDH as a loading control despite the fact that GAPDH expression has been reported to vary between sexes[41] with a higher stability across development in females.[42] This limits the use of GAPDH as a loading control. However, in our samples GAPDH expression was homogenous with 83% less than one standard deviation from mean and overall within two SD (mean = 1.08; SD = 0.13) and potential interference due to sex differences could be neglected. For raw data of GAPDH expression see Table 1.

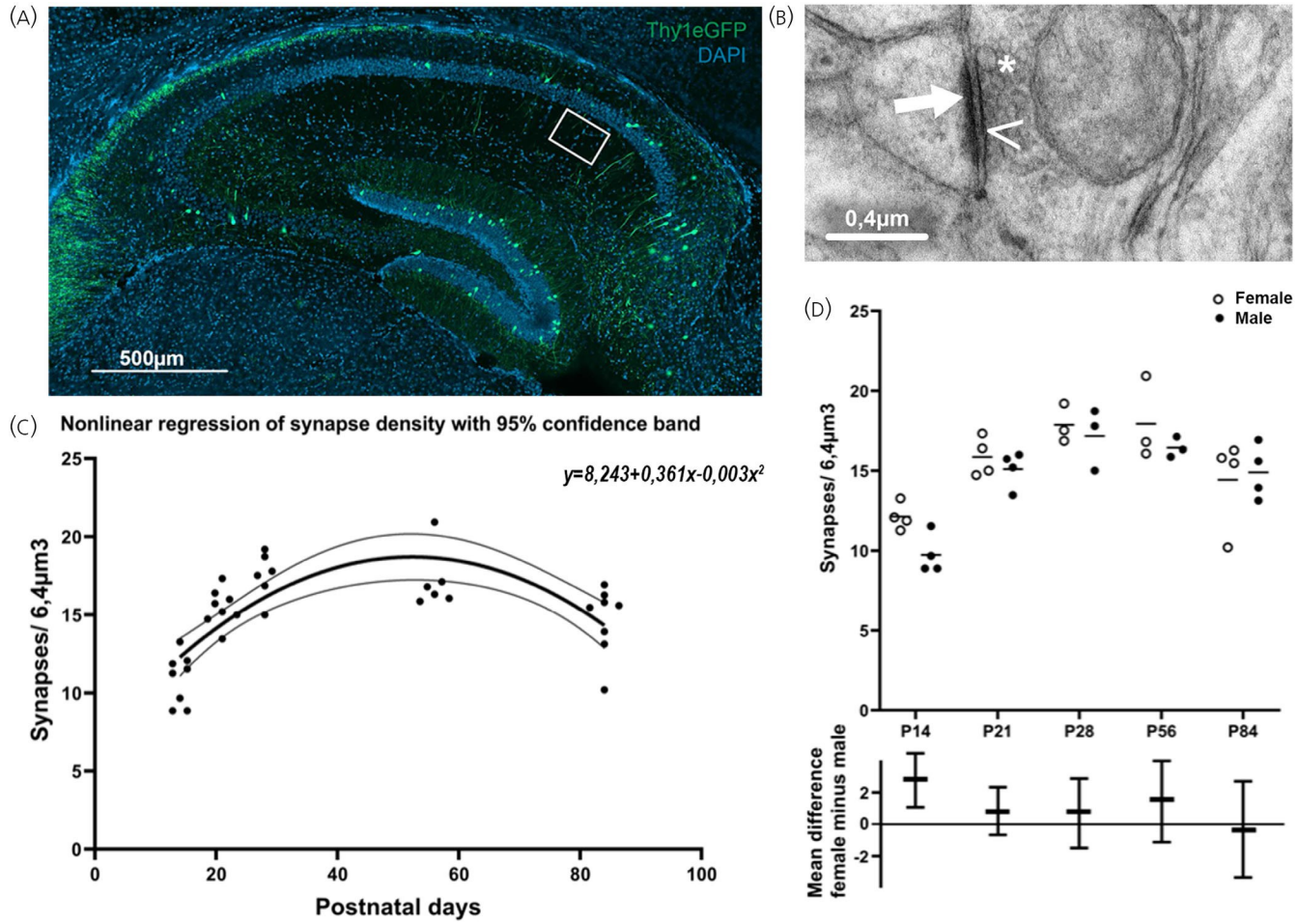

FIGURE 1Changes in synapse numbers are determined by age, but not sex, and synapse numbers are elevated in females at P14 only.

(A) Immunofluorescence overview of the hippocampus. The white box marks the region of interest in the stratum radiatum of the CA1 region.

(B) For each animal 15 neuropil fields with a volume of 6.4 µm^3 were stereologically investigated to examine synapse density in the hippocampus.

Only synapses with visible postsynaptic density !, presynaptic membrane <, synaptic cleft and postsynaptic membrane were counted.

Presynaptic vesicles * were considered facultative. (C) Nonlinear regression shows that changes in synapse density are determined by age. From the second to the fourth week a rise in synapse numbers, followed by a plateau phase and finally slow gradual loss up to 12 weeks can be found, with no difference between the sexes (adjusted R^2 = 0.475; F(3) = 9.651; p = .0001; SC Age = 3.971; SC Age^2 =3.822; p = .0001, n = 36; thin lines display the 95% confidence band). (D) The number of hippocampal CA1 spine synapses is greater in females than in males at P14, during the period of peak pruning. (Student's t-test; p = .02; mean difference = 2.38; 95% CI [0.83; 3.6]; Cohen's d = 2.229; n = 4).

The upper plot presents datapoints for single individuals, the lower plot visualizes effect sizes with vertical lines for the 95% CI of the mean

difference between groups.

2.6 | Statistical analysis

Statistical analysis was executed with SPSS 27 for Windows. Each dataset was checked for normal distribution with the Shapiro–Wilk test and datasets for ANOVA were checked with the Levene test for homogeneity of variance. Residuals of the dataset used for the regression model were examined for normal distribution and homoskedasticity and variables were centered to prevent multicollinearity. For each normally distributed dataset 95% confidence intervals, mean differences and effect strength are provided. For the regression model and chi-squared test post hoc power analyses were performed with G*Power. Data is presented as individual values with mean and mean differences visualized with a 95% confidence interval to illustrate effect size; the data of the contingency chart for spine contacts is presented as percentage bars. Data plots were visualized with Graphpad Prism 9.

Significant differences were defined at $p < .05$. p-values were controlled for a false discovery rate of $Q = 0.1$ with the BenjaminiHochberg procedure to prevent α error accumulation. With fdr = 0.1, no result with a 95% CI of the mean difference excluding zero had to be rejected as false positive. This leaves no risk of falsely rejecting an important finding, but also emphasizes the preference of the report of effect sizes and uncertainty as displayed in the visualization of the data (see Tables 2, 3 and 4).

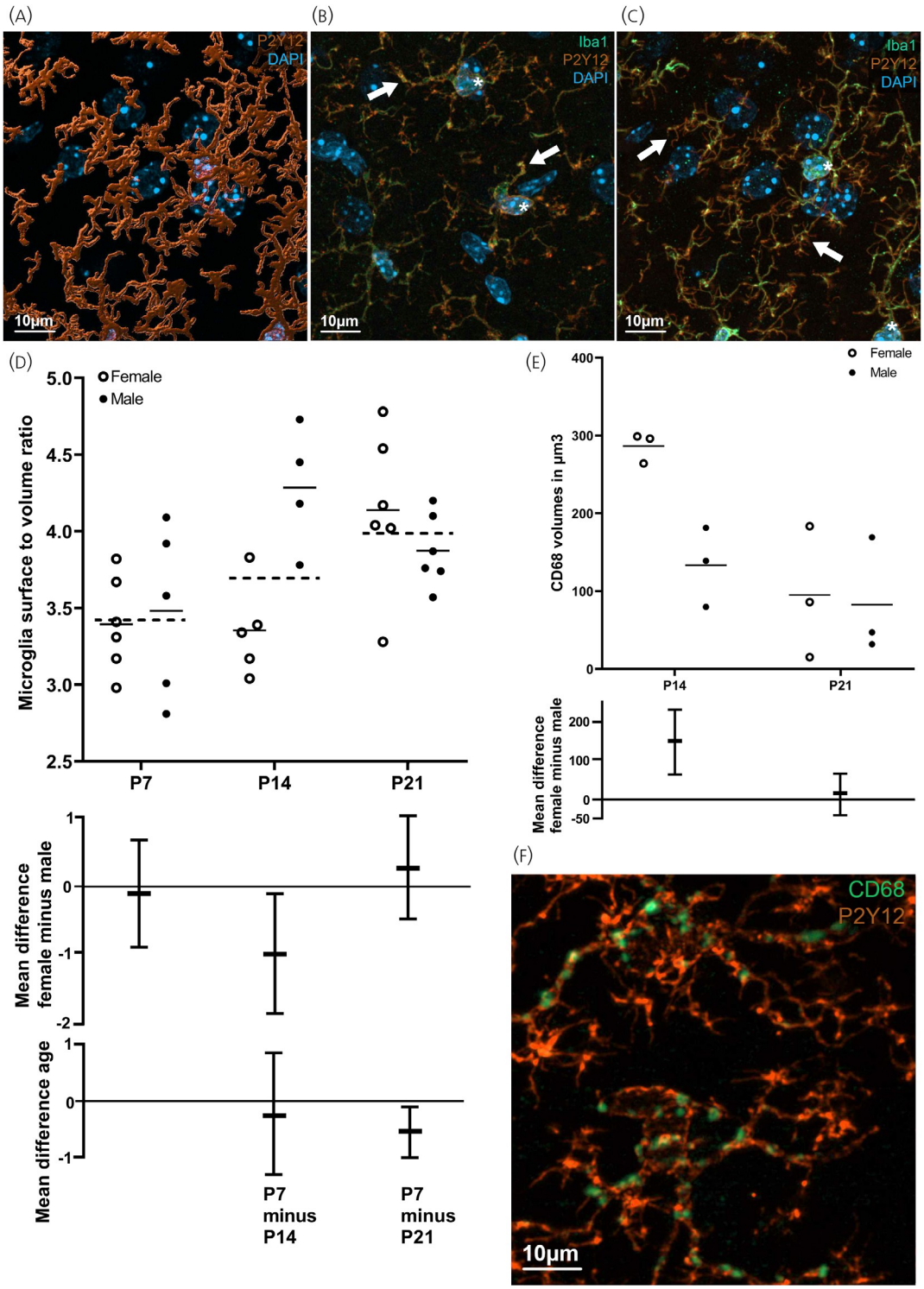

FIGURE 2Legend on next page.

3 | RESULTS

3.1 | Synapse density in the postnatal male and female hippocampus

We studied synaptic connectivity using electron microscopy by the determination of synaptic contacts rather than single spines or boutons,

which are not necessarily connected[21,43] as in Weinhard et al.[21] Dendritic spine counting is not necessarily indicative of synaptic connectivity, since not all spines, in particular the immature highly transient long spines, contact a bouton.[44–47]

We determined spine synapse density in the stratum radiatum of the hippocampal CA1 in male and female mice (Figure 1A). The synapses were defined by a bouton, a synaptic cleft, a post-synaptic density and a spine (Figure 1B). Altogether, hippocampi of 36 animals were used for a After counting, a nonlinear regression model was applied. The comprehensive comparison. Synapse density of the stratum radiatum model depicts that synapse density is significantly determined by age, of CA1 was determined using unbiased stereological counting.[48] but not by sex, with an average increase of 0.361 synapses per day

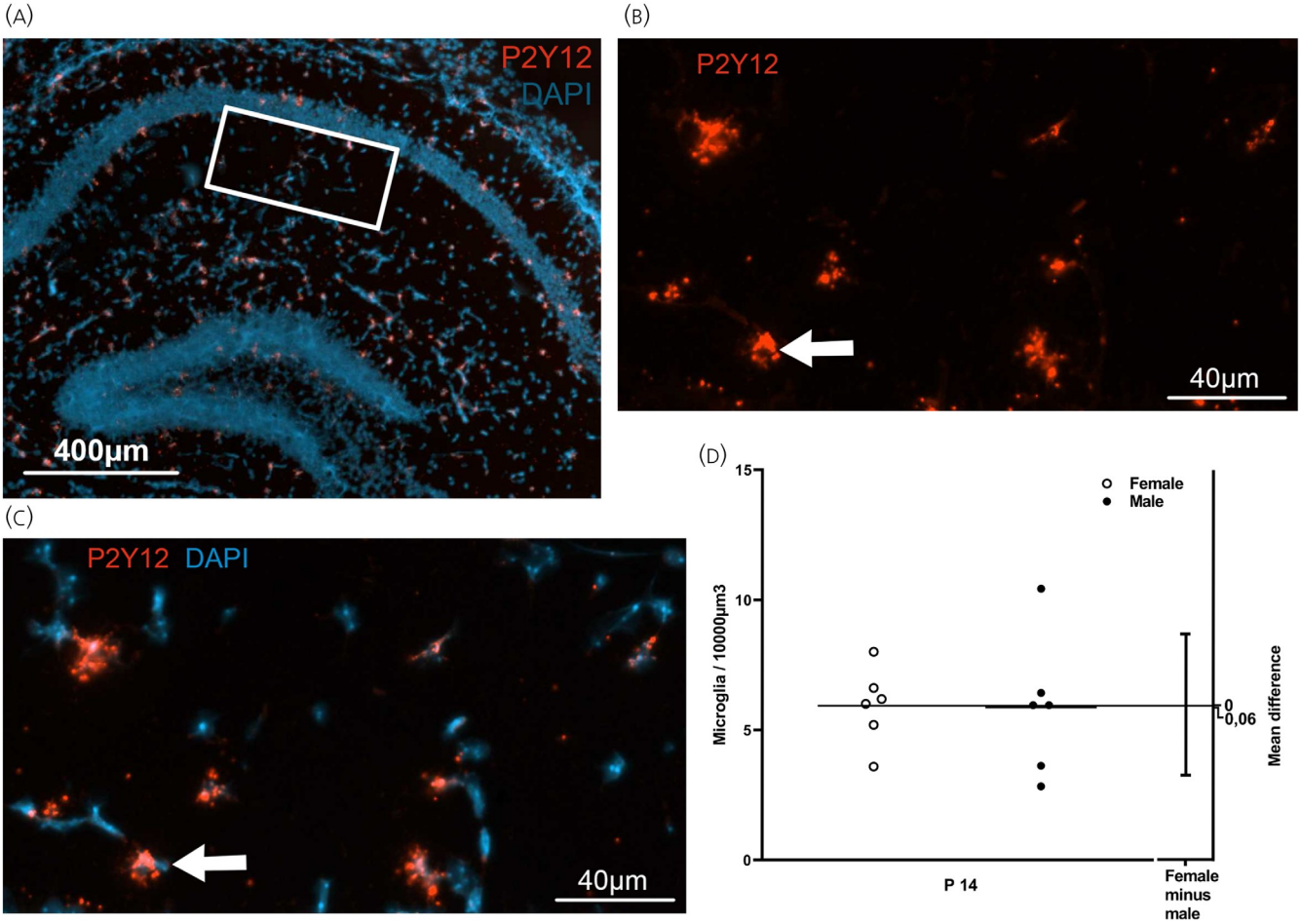

FIGURE 3 No sex specific difference in microglia colonization at P14. (A) Microglia cells were quantified with RNA Scope in planes of the stratum radiatum in the CA1 region with an average size of 75,480 µm^2. (B) P2Y12 RNA was detected with in situ hybridization. (C) P2Y12 signals were colocalized with DAPI to identify microglia nuclei. (D) There was no difference in the colonization of microglia at P14 (female–male mean difference = 0.066; 95% CI [2.7; 2.83]; SE = 1.24; p = .96). On the right verge of the plot, horizontal lines represent the mean difference, and the horizontal bar visualizes the 95% CI of the mean difference.

FIGURE 2 Developmental regulation of microglia is delayed in females and CD68 volume is elevated in females at P14. (A) Assessment of surface to volume ratio allows for microglia classification

without single cell categorization. Example image of three-dimensional microglia reconstruction used for determination of microglial morphology (overlay with DAPI). (B) Example image of microglia (P2Y12 colocalized with Iba1 and DAPI) with thick long processes , large somata *, and low surface to volume ratio (3.07). (C) Example image of microglia with thin ramified processes , smaller somata *, and high surface to volume ratio (4.78). (D) Low surface to volume ratio depicts a more spherical cell morphology, while a higher ratio means microglia are more ramified. At P7, microglia of both sexes show a stout morphology with thick long processes, but at P21 female and male microglia are ramified. At P14 a sexual dimorphism can be found with female microglia expressing a morphology similar to P7 and male microglia already showing the surface to volume ratio of microglia at P21. Because of insufficient staining, four datapoints from four different animals were excluded, accounting for a higher uncertainty of the P14 female–male mean difference (estimation plot with means of the individual groups as solid lines and means of age groups as dotted lines). Mean difference and 95% CI for age and sex are separately depicted below the data plot. ANOVA: $F(5) = 4.99$; $p = .002$ $\eta^2 = 0.49$ with Bonferroni method post hoc testing between groups: P7–P21 mean difference =0.57; 95% CI [1.0; 0.14]; SE = 0.17; $p = .008$; P14 female–male mean difference =0.93; 95% CI [1.8; 0.05]; SE = 0.27; $p = .03$). (E) CD68 volume is significantly higher in female microglia than in male at P14, substantiating a higher rate of engulfed particles processed in microglia at this point of time (ANOVA with planned contrast P14; $\eta^2 = 0.115$; mean difference = 152.98; SE = 31.5; 95% CI [65.53; 240.42]; $p = .008$; $n = 3$). The upper plots of (D) and (E) present datapoints for single individuals, the lower plots visualize effect sizes with vertical lines for the 95% CI of the mean difference between groups. (F) Example of a z-stack image of CD68-positive lysosomal granula (green) exclusively located in microglia (P2Y12/red).

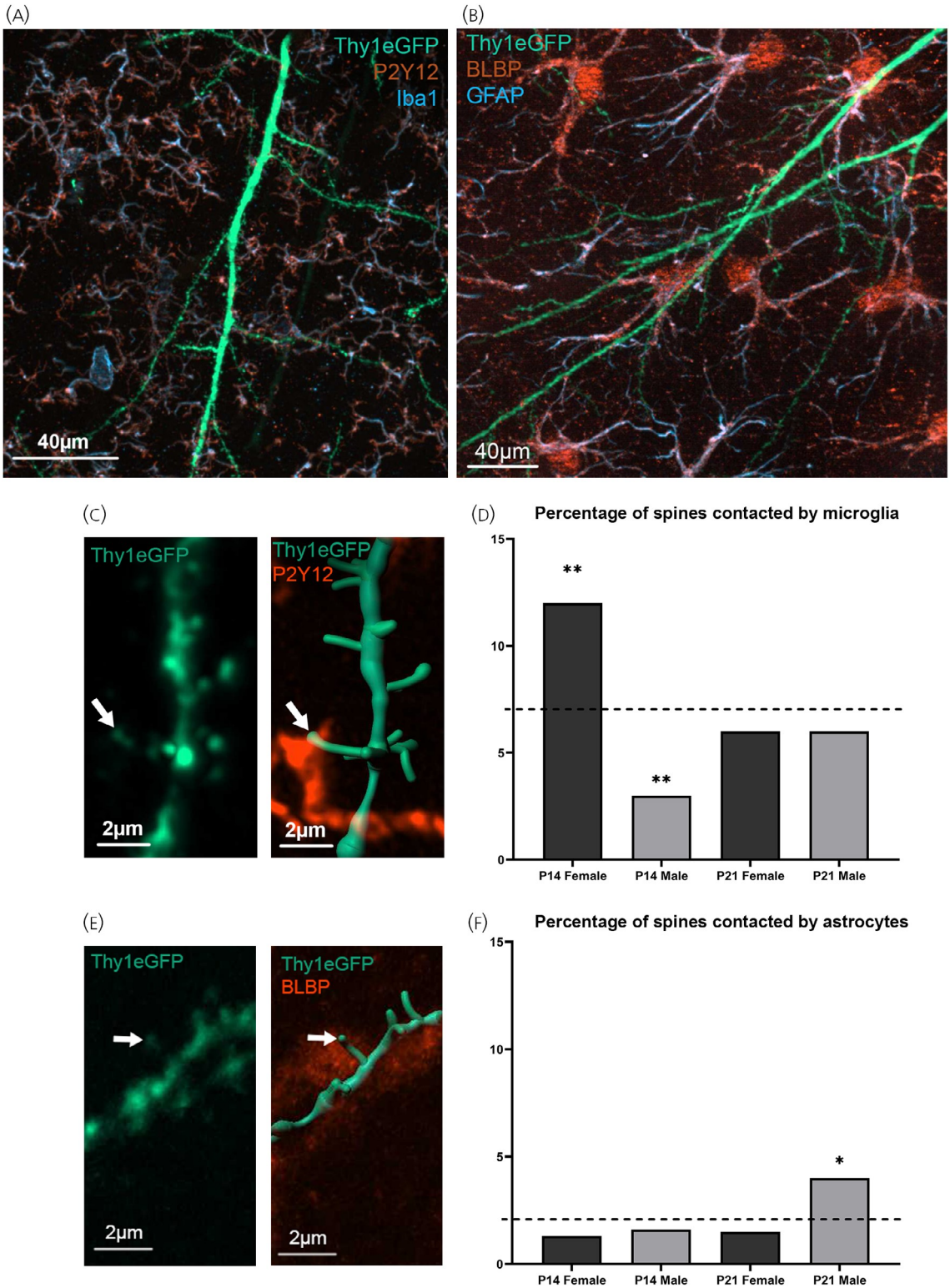

FIGURE 4Legend on next page.

followed by a loss of 0.003 synapses per number of days squared, which means there is a continuous rise in synapse density until the fourth week, followed by a plateau phase, and finally slow, gradual loss of synapses from the eighth week onwards. With an adjusted $R^2 = 0.475$ (equivalent to Cohens $f^2 = 0.77$) the model has a high quality and describes a strong effect with high significance ($p = .0001$). It should be noted in this context that this model does not allow for the prediction of synapse density beyond 12

weeks (adjusted $R^2 = 0.435$; $F(3) = 9.651$; $p = .0001$; SC Age = 3971; SC Age^2 =3822 $p = .0001$, $n = 36$) (Figure 1C).

Even if the course of synaptic remodeling was not different between males and females, and we did not find sex-specific differences in synapse densities in our regression model, a subgroup analysis revealed a higher synaptic connectivity in the female hippocampus at P14 (Figure 1D). This approach appeared to be justified, since hippocampal synaptic pruning is commonly described to appear during this early period of life.[10,21,49,50] With the selected assessment of synapse density at P14, we studied synapse density in relation to microglia number and microglia activity in this particular time window.

3.2 | Sex differences in microglia activity in the second postnatal week

In order to further assess microglia morphology and activity during the critical time window of the second postnatal week, we compared microglia at P7, P14, and P21.

Microglia show an amoeboid "stout" shape in an activated state and a ramified morphology when they are less active or in a quiescent state.[13,51] These cells, for instance, when conducting synaptic pruning in the dorsolateral geniculate nucleus, exhibit a specific morphology, characterized by thick long processes and large cell bodies. This morphology is accompanied by strong expression of CD68, which is indicative of phagocytotic processes.[52] We thus tested CD68 expression and determined surface to volume ratios of microglia in the time window of interest.

Activated microglia with thick processes and large somata (Figure 2B) show a low surface to volume ratio, while microglia with lots of thin, ramified processes show a high surface to volume ratio (Figure 2C). For the determination of surface to volume ratios, microglia were three-dimensionally reconstructed (Figure 2A).

Cell morphology differed significantly regarding sex and age. P7 microglia show lower surface to volume ratios than P21 microglia, due to ramification during this period.

At P14 a sexual dimorphism was found, with female microglia expressing a morphology similar to P7 and male microglia showing the surface to volume ratio of microglia at P21 (ANOVA: P7–P21 mean difference = 0.57; SE = 0.17; $p = .008$ P14 female–male mean difference = 0.93; SE = 0.27; $p = .03$; Figure 2D). Confirming previous studies,[21] microglia of females are more activated than microglia of males at P14.

Consistently, CD68-positive lysosomal granules (Figure 2F), which are commonly associated with microglial activation,[19,53] were detected in an immunofluorescence and 3D reconstructed assay. CD68 volumes were significantly elevated in females at P14 (ANOVA; P14 female– male mean difference = 152.98; SE = 22.27; $p = .008$ Figure 2E).

Differences in the colonization of the hippocampus of microglia did not account for sex-dependent differences. The number of microglia was not changed at P14 (Figure 3). We also tested the potential involvement of astrocytes. Even though astrocytes contacted spines more frequently in males at P21, compared with microglia the ratio of these contacts was very low and may be neglected (Figure 4E).

3.3 | Sex differences in spatial relationships of microglia and synaptic sites in the second postnatal week

To focus on microglia action in more detail we used Thy1-GFP transgenic mice, in which GFP is expressed only in subpopulations of neurons and thus allows the counting of selectively spines or selectively boutons in hippocampal vibratome sections on the light microscopical level. In sections of P7, P14 and P21 animals we performed immunohistochemistry of P2Y12, as a marker of microglia, and we studied the staining in relation to the eGFP-labeled spines (Figure 4A). Unfortunately, in P7 mice, the eGFP labeling was not strong enough for the identification of individual spines. First order dendrites in the hippocampal region CA1 were chosen for the detection of double labeling that is eGFP and P2Y12. We found P2Y12 immunoreactivity in

close vicinity of eGFP-labeled spines, thus potential synaptic contacts (Figure 4C). In Thy1-GFP mice adjacent boutons are not necessarily stained, since only selected neurons are GFP labeled. The contacts between spines and microglia were quantified. We found a four-fold

FIGURE 4 Microglia spine contacts are fourfold higher in females at P14. (A) Hippocampal pyramidal neurons located in the CA1 region of mice of two and 3 weeks of age from both sexes were used for immunofluorescence. Z-stack images of at least 10 µm thickness were obtained with a Zeiss Apotome 2 (Thy1-eGFP: green; P2Y12: red; Iba1: blue). For each neuron, one region of interest including a first order dendrite with an average length of 64 µm was chosen for 3D reconstruction with Oxford Instruments Imaris. (B) For the analysis of astrocyte spine interactions, z-stack images were acquired in a similar way from the CA1 region (Thy1-eGFP: green; BLBP: red; GFAP: blue) (C) Example image of microglia encapsulating a three-dimensionally reconstructed dendritic spine. (D) Out of 2234 spines, 150 were contacted by microglia. To examine whether the findings of sex specific differences in microglia morphology would affect microglia spine interactions, spines were categorized for sex and age (P14 female, P14 male, P21 female, P21 male), and the rate of microglial contacts was assessed for each category. Female spines were fourfold more highly contacted by microglia than male spines at P14. Pearson's chi-square test was applied and showed significance ($\chi^2(3) = 29.06$; Cramer's $V = 0.114$; $p = .0001$). Post hoc tests revealed significance for the sex dependency of contact frequency at P14, with a higher rate of contacts for female spines ($p = .0001$; Cramer's $V = 0.1$) and a lower rate of contacts for male spines ($p = .0003$; Cramer's $V = 0.09$). Bars of the graph show the percentage of encapsulated spines per category with a dotted line depicting the expected value and stars indicating significant deviation from it. (E) Example image of astrocyte contacting a three-dimensionally reconstructed dendritic spine. (F) Out of 1682 spines, 36 were contacted by astrocytes. Spines were again categorized by sex and age and Pearson's chi-square test showed significance for the elevated contact frequency in males at P21 ($\chi^2(3) = 10.841$; Cramer's $V = 0.08$; $p = .015$). Bars of the graph show the percentage of contacted spines per category with a dotted line depicting the expected value and stars indicating significant deviation from it.

FIGURE 5 Presynaptic bouton density is elevated in females at P14, but spine density and spine type distribution are not different at P14 and P21. (A) Presynaptic bouton density in CA3 axons is elevated in females at P14 (Student's t-test; $p = .03$; mean difference = 5.6; 95% CI

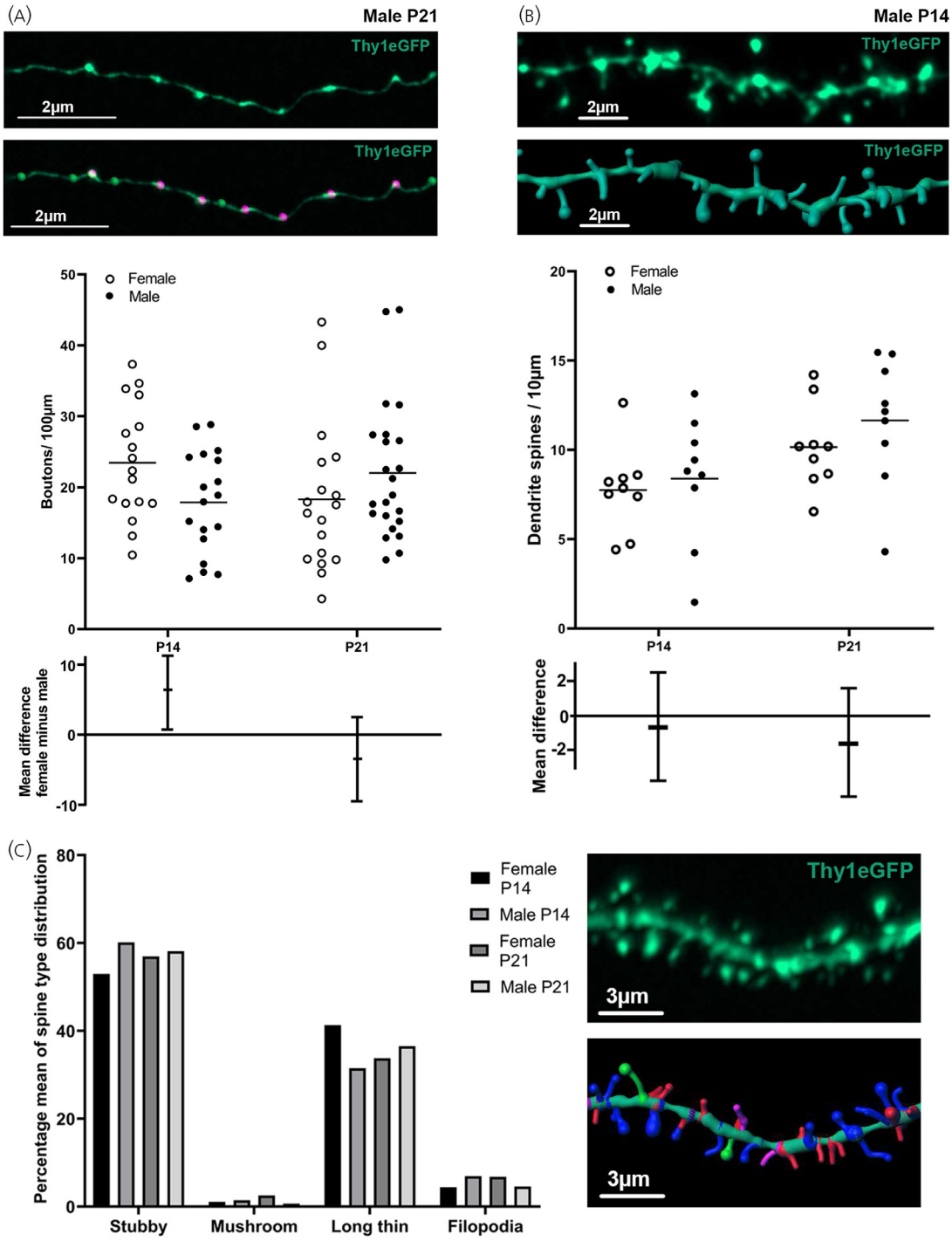

[0.37; 10.84]; SE = 2.57 Cohen's d =0.374). A total of 78 axons with an average length of 64.5 µm were analyzed for bouton density with Imaris. Boutons were counted positive when the bouton intensity (magenta spheres) exceeded the intensity of the axon shaft (green spheres) by at least 40% (1–6 cells per animal, n = 3 animals, P21 female–male mean difference =3.73; 95% CI [10.1; 2.62]; SE = 3.14; p = .24). (B) There was no difference in spine density between P14 and P21, indicating that spine density does not reflect synaptic density (average dendrite length 64 µm, 3 cells per animal, n = 3 animals, P14 female–male mean difference =0.63; 95% CI [3.67; 2.41]; SE = 1.55; p = .66; P21 female–male mean

difference =1.49; 95% CI [4.53; 1.55]; SE = 1.55; p = .31). The upper plots of (A) and (B) present datapoints for single individuals, the lower plots visualize effect sizes with vertical lines for the 95% CI of the mean difference between groups. (C) Three dimensional reconstructed spines were classified into stubby (red), long thin (blue), mushroom (green) and filopodia (purple) by using the Imaris Classify Spines Xtension. Spines were classified as stubby spines based on spine length and mushroom or thin long spines based on head/neck ratio. Spines with a length greater than 1 μm and smaller head than neck width were categorized as filopodia. Spine type distribution means are generally similar when categorized for sex and age.

higher percentage of close contacts in sections of females than in sections of male animals at P14 (Figure 4D).

The close contacts between microglia and eGFP-positive synaptic structures prompted us to further determine spine and spine type density and bouton density. We found differences regarding bouton density (Figure 5A). At P14 we found significantly more boutons in females than in males, which was consistent with increased synapse density in females at this time point. At P21, however, bouton number decreased again, despite the increase in synapse numbers, and this suggests the formation of multispine boutons (MSB). Surprisingly, and in contrast to the study by Weinhard et al.,[21] we did not find any difference between males and females at P14, regarding spine density (Figure 5B). This might be due to the fact that the lateral pixel size of the obtained images was lower (160 nm as compared to 40 nm by Weinhard et al.[21]). Therefore, the threshold for spine head diameters had to be set to 0.3 µm to avoid false positive detections, which might cause a false low number of detected filopodia (Figure 5C).
The limitations of fluorescence microscopy have been addressed previously in other studies.[54]

3.4 | CD47 expression is similar in the male and female P14 hippocampus

CD47 expression and signaling prevents excess microglial phagocytosis during developmental synaptic pruning. CD47 is required for neuronal activity-mediated changes in microglial engulfment and CD47 serves as a “don't eat me” signal.[55] As a final step, we studied CD47 expression in neurons of P14 hippocampus, but detected no difference in the expression of male and female hippocampi when using western blot analysis (Figure 6).

4 | DISCUSSION

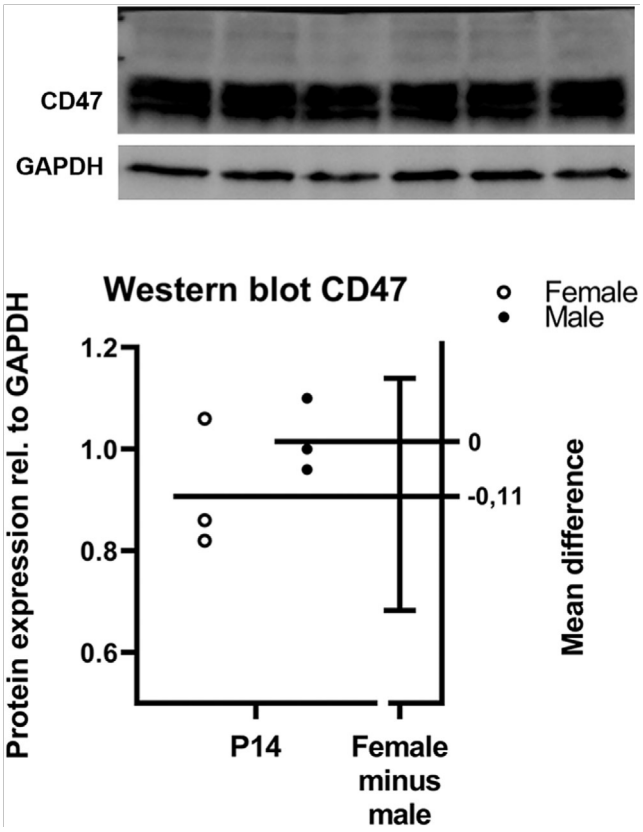

FIGURE 6 No sex specific difference in CD47 expression at P14. CD47 is considered a "don't eat me" signal for microglia and protects functional synapses from pruning. This marker was examined by western blot to investigate if the excess number of synapses in females at P14 is a sign of earlier maturation than in males (which would be shown by a relatively higher expression of CD47 in females). No difference in the relative CD47 to GAPDH expression between the sexes can be found at P14. On the right verge of the plot, horizontal lines represent the mean difference, and the horizontal bar visualizes the 95% CI of the mean difference.

Our determination of synaptic density in electron micrographs during the postnatal period revealed no sex specificity in the dynamics of synaptic connectivity. An initial increase in synapse numbers after birth was followed by a continuous decrease up to adulthood with no difference between sexes. Temporarily, only at P14, during the rise of synapse numbers, was higher synapse density in females than in males accompanied by stronger microglia activity in females than in males, which supports the role of microglia in synaptic refinement. Overall, sexual differentiation of microglia does not contribute to the developmental dynamics of synaptic connectivity from birth to adulthood.

4.1 | Dynamics of synapse development from birth to adulthood

In the hippocampus, like in other regions of the brain, synapse numbers initially increase and decrease thereafter over the course of postnatal development. This was shown for the first time by Feinberg[56] almost 50 years ago. Rakic et al.[1] studied synapse density in the cortex of monkeys using electron microscopy. Since then, the majority of studies have focused on postsynaptic spine development and used spine development as indicative of synapse formation. Spines, however, are not necessarily connected with boutons, and spine density is

not always identical with synapse density.[57] For the first time, to the best of our knowledge, our study presents synapse development during the postnatal period using stereological counting of synapses at the ultrastructural level, and applies a statistical model to assess the dynamics of synaptic connectivity during the postnatal period.

Based upon this model, our data confirm a period after birth when synapse formation dominates synaptic pruning followed by a net loss of synapses as the rate of pruning, very slowly but exponentially, overtakes that of synapse formation, with no differences between males and females.

It has been frequently shown that the loss of synapses is required for the refinement and proper functioning of neuronal circuits: disruption of synapse pruning can lead to dysfunction underlying some neurodevelopmental and psychiatric disorders[58,59] in particular, disorders in the autism spectrum.[60–62]

The idea of synapse pruning as a function of exclusive microglia action may be challenged by microglial numbers during the postnatal period. Nikodemova et al.[63] found that microglial numbers increase within the first two postnatal weeks and decline in the third postnatal week. By 6 weeks the numbers were reduced by 50%, which was maintained up to adulthood. In our study, loss of synapses was slow and gradual, consistent with the findings of Rakic et al. and Feinberg.[1,56] The development of synapse density suggests that the formation of synapses dominates elimination of synapses during the first postnatal weeks, with synaptic pruning dominating synaptogenesis, thereafter, starting at 4 weeks postnatally. Thus, the switch takes place shortly before the maximal decline in microglia numbers, suggesting other mechanisms underlying synapse loss during adolescence and puberty. This is underlined by the findings of Weinhard et al.[21] After 4 weeks, Weinhard and coworkers described higher activity of microglia in males than in females. However, we found no difference in synapse numbers between sexes after 4 weeks postnatally, when reduction of synapse numbers becomes particularly evident.

For the future, it will be important to consider more thoroughly the role of astrocytes in juvenile synaptic pruning, as shown in adults by Lee et al.,[4] even if our findings only suggest a minor, if any, role of astrocytes in postnatal synaptic pruning. However, Du et al.[64] postulated that astrocytes play a role in synaptic pruning, which is eventually mediated by microglia. Using TREM2 deficient mice, it has been shown that microglia instruct synaptic elimination by astrocytes during neurodevelopment.[65] Finally, the role of autophagy in neurons and a potential interplay with glial phagocytosis needs to be addressed with respect to synaptic pruning.[66] Autophagy plays a crucial role in differentiation by promoting cell remodeling including cytoskeleton and membrane receptor degradation as well as organelle degradation.[67–69] Neurons have a higher level of autophagic flux than other cell types, which underscores the importance of autophagy for the maintenance of homeostatic balance and neuronal function. In this context, there is also evidence that synaptic pruning is regulated by autophagy. For example, in brains of autism spectrum disorder patients synaptic pruning was reduced, and the reduced synaptic pruning was inversely associated with autophagy marker.[62,70]

4.2 | A bidirectional role of microglia: In synaptogenesis and in synaptic pruning

The development of synaptic connectivity from birth to adulthood includes the elimination of redundant, weak synapses, but also the formation of new synapses. In both processes, microglia play an essential role; in other words microglia have bidirectional functions. In our study, we found an increase in synapse density up to 4 weeks and a continuous decrease in synapse density up to adulthood in males as well as in females. Microglia contribute to

synaptogenesis by inducing the formation of filopodia[9,12,71] as well as to synaptic pruning, by engulfing redundant synaptic material.[10,21,72]

The group of Cornelius Gross[10] showed that synaptic pruning, and thereby the remodeling of the brain during the period from birth to adulthood, is a function of microglia. They postulated that microglia engulf synaptic material. In this context, however, it needs to be mentioned that the data were generated by using immunohistochemical staining of synaptic proteins, such as PSD95, a protein of the postsynaptic density and SNAP 25, a presynaptic protein involved in transmitter release, to assess synaptic connectivity. They found PSD95 or SNAP25 puncta in vesicles within some microglial processes, suggestive of synapse engulfment. This was questioned in the study by Weinhard et al.[12] who did not find evidence that microglia engulf postsynaptic material and instead provided evidence on an elaborative ultrastructural level that presynaptic material is partly eliminated but not spines. The role of microglia in synaptic pruning was substantiated by a recent study on the role of microglia shortly after birth. They ablated microglia on P7 and found an increase in CA1 mature neurons at P14.[73]

An active role of microglia in synaptogenesis was first described by Parkhurst et al.,[71] who demonstrated a reduction in motor-learning-dependent synapse formation in mice depleted of microglia and later on by Miyamoto et al.,[9] who by using in vivo multiphoton imaging showed that microglia contact to dendrites induced the formation of filopodia in the somatosensory cortex. The formation of filopodia was abolished after depletion of microglia. The microglia contactinduced filopodia formation was a transient phenomenon and was observed in P8–P10 mice and corresponded to the amoeboid, activated state of microglia. Potential differences between sexes were not considered. In our study, which was focused on sex-specific effects, we found no change in the activity of microglia in male and females at P7. At P14, however, we found increased activity of microglia in females as compared to males, together with increased synapse numbers in females, which confirms the transient character of microglia activation in females. From the findings by Miyamoto et al.[9] it appears that filopodia formation between P8–P10 precedes synapse formation at P14, as seen in our study.

The bidirectional role of microglia was most elegantly shown by Weinhard et al.[12] Aside from partial pruning of boutons, they found spine filopodia at sites of microglia-bouton contacts and proposed an active role of microglia in the remodeling of connectivity, by formation of premature spines, which would, in principle, identify postnatal synaptogenesis and postnatal synaptic pruning as simultaneous processes.

4.3 | Microglia and synaptic multiplicity

The decrease in female bouton numbers despite increase in synapse numbers between P14 and P21, suggests that microglia-induced filopodia, as described by Weinhard et al.[12] and Miyamoto et al.,[9] have contact to pre-existing boutons at P14 to form mature synapses. This is consistent with the observation that microglia-induced filopodia integrate into neuronal circuits since ablation of microglia reduced the frequency of excitatory synaptic transmission.[9,11] Furthermore, Zhan et al.[11] investigated the effects of microglia depletion on synaptic multiplicity (number of synapses per axonal input) and demonstrated that microglia in juvenile mice are necessary for the establishment of multispine boutons (MSB). Formation of MSBs could account for the decrease in female bouton numbers between P14 and P21, although synapse numbers increased during this period. The lack of MSBs caused by microglia depletion resulted in diminished whole cell EPSCs.[11] In an earlier study, Toni et al. had already shown that MSBs become sites for the synthesis of new synapses, which would strengthen established connectivity.[74] Consistent with these findings, Weinhard and coworkers

found microgliainduced filopodia formation starting on the heads of existing spines. In addition, they demonstrated that microglia relocate spine heads to the tips of the newly induced spine filopodia. These spineheads are then reconnected to different axonal boutons by microglia.[12,21] The genesis of new synapses in MSBs could account for the overall increase in synapse density we found until the fourth week. Since we found an increase in synapse numbers, but a decrease in bouton numbers between P14 and P21 in both sexes, it appears that the establishment of synaptic multiplicity, that is MSBs, as described by Zhan et al.,[11] preferentially takes place during this timeframe. In addition, our observation that synapse and bouton numbers are elevated in females at P14 compared to males, suggests a temporal shift in this process between both sexes.

4.4 | Sexual differentiation of microglia

During the last decade, increasing evidence has emerged that microglia are involved in sex-specific processes of differentiation in the brain[14–17] The relationship between sex, glia and brain development was first chosen as a central theme by Schwarz et al.[75] and Schwarz and Bilbo,[76] with their studies on sex differences in microglial colonization of the developing rat brain.[13,77,78] Before birth, males appear to have more microglia than females. Ruggiero et al.,[78] showed that the number of microglia in males and females did not differ on P8 as females added a significant number of microglia to all subregions of the hippocampus during this period. This is consistent with our data using the RNA scope and showing no differences in microglial numbers in CA1 at P14 between female and male animals.

Many studies have uncovered sex differences of rodent microglia regarding antigen presentation, phagocytic capacity, responsiveness to radiotherapy and exogenous stimuli and finally epigenetic control (for review see[79]). Amazingly, as yet, no comprehensive studies exist regarding the expression of steroid receptors during development.[22,80] Sex steroid concentrations in the tissue and in serum are similar during the early postnatal phase,[81] thus the equipment of microglia with steroid receptors could be a regulatory mechanism with respect to sex differences. Recent studies used RNA sequencing technologies to detect transcriptional and translational differences of microglia from male and female brains and found differences between sexes,[16,77] while Hammond et al.,[82] did not find any sex differences in the transcriptomes. Microglia isolated from males showed a developmental delay as compared to females, when comparing embryonic microglia with microglia from p60 animals. Unfortunately, the time window of the first two postnatal weeks, which would allow the discussion of our data, was not considered in any of the cited studies (for review see[14]). Differences seen at P14 may in part underlie some of the well-known sex differences underlying neurodevelopmental outcomes.[83] For instance, it has been shown that early life inflammation increases CA1 pyramidal neuron excitability in a sex and age dependent manner.[84] Our results, however, confirm the second postnatal week as a close time window of sex specific differences in microglia-induced synaptic refinement.[21,63,77]

Sex-specific differences in microglia activity parallels sex-specific differences in synapse density in the hippocampus. As compared to male microglia, there appears to be a delay in the development of microglia in females between P7 and P21 leading to the observed difference in synaptic numbers at P14. Considering the higher level of phagocytosis marker CD68, presynaptic bouton numbers, and morphological differences of microglia in females at P14, it appears that microglia of newborn females engulf synapses at a slower rate based on lower phagocytotic capacity shortly after birth and that the pruning process after birth in females is initiated later than in males. On the one hand, the higher level of phagocytosis marker CD68 in female microglia at P14 together with the higher number of synapses in females at this developmental stage make a developmental delay in females likely, with female microglia

catching up phagocytosis to reach male synaptic levels again at P21. It is of note that sex specific differences in microglia between male and females up to adulthood[21,63,73] do not result in overall changes in synapse numbers, as soon as the developmental delay has caught up. On the other hand, considering the role of activated microglia in the establishment of an adult network by promoting synapse formation, we cannot exclude that differences in synapse densities in females may additionally result from enhanced synaptogenesis induced by microglia, for example, by facilitating development of MSBs.

The reason for the upregulation of microglia selectively at P14 in females as compared to males, however, remains to be clarified and needs further investigation. Overall and most importantly, despite the important role of microglia in synapse remodeling, sexual differentiation of microglia does not result in long lasting sex differences in the developmental dynamics of synaptic connectivity from birth to adulthood.

AUTHOR CONTRIBUTIONS

Tim M. Prengel: Data curation; formal analysis; investigation; visualization; writing – original draft; writing – review and editing. Bianka Brunne: Conceptualization; methodology; supervision; writing – review and editing. Moataz Habiballa: Methodology. Gabriele Maria Rune: Conceptualization; formal analysis; project administration; resources; supervision; validation; writing – original draft.

ACKNOWLEDGMENTS

We wish to thank Dr Zhou for experimental help and Liz Grundy, Theres Schaub, and Mateusz Ambrozkiewicz for reading the manuscript. Finally, we would like to thank Alina Jahrmarkt for contributing to the design of the figures. Open Access funding enabled and organized by Projekt DEAL.

FUNDING INFORMATION

The study was supported by the Deutsche Forschungsgemeinschaft (DFG 436/7-1).

CONFLICT OF INTEREST STATEMENT

The authors declare that they have no conflict of interest.

PEER REVIEW

The peer review history for this article is available at https://www.webofscience.com/api/gateway/wos/peer-review/10.1111/jne.13276.

DATA AVAILABILITY STATEMENT

The data that support the findings of this study are available from the corresponding author upon reasonable request.

ORCID

Tim M. Prengel https://orcid.org/0000-0002-9753-0168

Gabriele M. Rune https://orcid.org/0000-0003-3378-4684

REFERENCES

1. Rakic P, Bourgeois JP, Eckenhoff MF, Zecevic N, Goldman-Rakic PS. Concurrent overproduction of synapses in diverse regions of the primate cerebral cortex. Science. 1986;232(4747):232-235.
2. Ueno M, Yamashita T. Bidirectional tuning of microglia in the developing brain: from neurogenesis to neural circuit formation. Curr Opin Neurobiol. 2014;27:8-15.
3. Stoneham E, Sanders E, Sanyal M, et al. Rules of engagement: factors that regulate activity-dependent synaptic plasticity during neural network development. Biol Bull. 2010;219:81-99.

4. Lee JH, Kim JY, Noh S, et al. Astrocytes phagocytose adult hippocampal synapses for circuit homeostasis. Nature. 2021;590(7847): 612-617.
5. Pinto B, Morelli G, Rastogi M, et al. Rescuing over-activated microglia restores cognitive performance in juvenile animals of the Dp(16) mouse model of down syndrome. Neuron. 2020;108(5):887904.e12.
6. Patel AB, Loerwald KW, Huber KM, Gibson JR. Postsynaptic FMRP promotes the pruning of cell-to-cell connections among pyramidal neurons in the L5A neocortical network. J Neurosci. 2014;34(9):34133418.
7. Horling K, Schlegel G, Schulz S, et al. Hippocampal synaptic connectivity in phenylketonuria. Hum Mol Genet. 2015;24(4):1007-1018.
8. Prinz M, Jung S, Priller J. Microglia biology: one century of evolving concepts. Cell. 2019;179(2):292-311.
9. Miyamoto A, Wake H, Ishikawa AW, et al. Microglia contact induces synapse formation in developing somatosensory cortex. Nat Commun. 2016;7:12540.
10. Paolicelli RC, Bolasco G, Pagani F, et al. Synaptic pruning by microglia is necessary for normal brain development. Science. 2011;333(6048): 1456-1458.
11. Zhan Y, Paolicelli RC, Sforazzini F, et al. Deficient neuron-microglia signaling results in impaired functional brain connectivity and social behavior. Nat Neurosci. 2014;17(3):400-406.
12. Weinhard L, di Bartolomei G, Bolasco G, et al. Microglia remodel synapses by presynaptic trogocytosis and spine head filopodia induction. Nat Commun. 2018;9(1):1228.
13. Forger NG, Strahan JA, Castillo-Ruiz A. Cellular and molecular mechanisms of sexual differentiation in the mammalian nervous system. Front Neuroendocrinol. 2016;40:67-86.
14. Bordt EA, Ceasrine AM, Bilbo SD. Microglia and sexual differentiation of the developing brain: a focus on ontogeny and intrinsic factors. Glia. 2020;68(6):1085-1099.
15. VanRyzin JW, Marquardt AE, Pickett LA, McCarthy MM. Microglia and sexual differentiation of the developing brain: a focus on extrinsic factors. Glia. 2020;68(6):1100-1113.
16. Villa A, Della Torre S, Maggi A. Sexual differentiation of microglia. Front Neuroendocrinol. 2019;52:156-164.
17. Arambula SE, McCarthy MM. Neuroendocrine-immune crosstalk shapes sex-specific brain development. Endocrinology. 2020;161(6): 1-13.
18. Kodama L, Gan L. Do microglial sex differences contribute to sex differences in neurodegenerative diseases? Trends Mol Med. 2019;25(9): 741-749.
19. Nelson LH, Lenz KM. The immune system as a novel regulator of sex differences in brain and behavioral development. J Neurosci Res. 2017;95(1–2):447-461.
20. Nelson LH, Saulsbery AI, Lenz KM. Small cells with big implications: microglia and sex differences in brain development, plasticity and behavioral health. Prog Neurobiol. 2019;176:103-119.
21. Weinhard L, Neniskyte U, Vadisiute A, et al. Sexual dimorphism of microglia and synapses during mouse postnatal development. Dev Neurobiol. 2018;78(6):618-626.
22. Nissen JC. Microglial function across the Spectrum of age and gender. Int J Mol Sci. 2017;18(3):561. doi:10.3390/ijms18030561
23. Nelson BS, Springer RC, Daniel JM. Antagonism of brain insulin-like growth factor-1 receptors blocks estradiol effects on memory and levels of hippocampal synaptic proteins in ovariectomized rats. Psychopharmacology (Berl). 2014;231(5):899-907.
24. Crespo-Castrillo A, Arevalo MA. Microglial and astrocytic function in physiological and pathological conditions: estrogenic modulation. Int J Mol Sci. 2020;21(9):3219. doi:10.3390/ijms21093219
25. Feng G, Mellor RH, Bernstein M, et al. Imaging neuronal subsets in transgenic mice expressing multiple spectral variants of GFP. Neuron. 2000;28(1):41-51.
26. Frotscher M, Heimrich B. Formation of layer-specific fiber projections to the hippocampus in vitro. Proc Natl Acad Sci U S A. 1993;90(21): 10400-10403.
27. Frotscher M, Heimrich B, Schwegler H. Plasticity of identified neurons in slice cultures of hippocampus: a combined Golgi/electron microscopic and immunocytochemical study. Prog Brain Res. 1990;83:323-339.
28. Sterio DC. The unbiased estimation of number and sizes of arbitrary particles using the disector. J Microsc. 1984;134(Pt 2): 127-136.
29. Woolley CS, McEwen BS. Estradiol mediates fluctuation in hippocampal synapse density during the estrous-cycle in the adult-rat. J Neurosci. 1992;12(7):2549-2554.
30. Leranth C, Shanabrough M, Horvath TL. Hormonal regulation of hippocampal spine synapse density involves subcortical mediation. Neuroscience. 2000;101:349-356.
31. Braendgaard H, Gundersen HJ. The impact of recent stereological advances on quantitative studies of the nervous system. J Neurosci Methods. 1986;18(1–2):39-78.
32. Prange-Kiel J, Rune GM, Leranth C. Median raphe mediates estrogenic effects to the hippocampus in female rats. Eur J Neurosci. 2004; 19:309-317.
33. Cserép C, Posfai B, Lénárt N, et al. Microglia monitor and protect neuronal function through specialized somatic purinergic junctions. Science. 2020;367(6477):528-537.
34. Lier J, Streit WJ, Bechmann I. Beyond activation: characterizing microglial functional phenotypes. Cell. 2021;10(9):236. doi:10.3390/cells10092236
35. Weigel A, Schild D, Zeug A. Resolution in the ApoTome and the confocal laser scanning microscope: comparison. J Biomed Opt. 2009; 14(1):014022.
36. Ma Y, Wen K, Liu M, et al. Recent advances in structured illumination microscopy. J Phys Photonics. 2021;3(2):024009.
37. Vuksic M, Del Turco D, Bas Orth C, et al. 3D-reconstruction and functional properties of GFP-positive and GFP-negative granule cells in the fascia dentata of the Thy1-GFP mouse. Hippocampus. 2008;18(4):

364-375.
38. Verstraelen P, Garcia-Diaz Barriga G, Verschuuren M, et al. Systematic quantification of synapses in primary neuronal culture, iScience. 2020;23(9):101542.
39. Basu S, Saha PK, Roszkowska M, et al. Quantitative 3-D morphometric analysis of individual dendritic spines. Sci Rep. 2018;8(1):3545.
40. Wang F, Flanagan J, Su N, et al. RNAscope: a novel in situ RNA analysis platform for formalin-fixed, paraffin-embedded tissues. J Mol Diagn. 2012;14(1):22-29.
41. Perrot-Sinal TS, Davis AM, McCarthy MM. Developmental sex differences in glutamic acid decarboxylase (GAD(65)) and the housekeeping gene, GAPDH. Brain Res. 2001;922(2):201-208.
42. Cheung TT, Weston MK, Wilson MJ. Selection and evaluation of reference genes for analysis of mouse (Mus musculus) sex-dimorphic brain development. PeerJ. 2017;5:e2909.
43. Kasthuri N, Hayworth KJ, Berger DR, et al. Saturated reconstruction of a volume of neocortex. Cell. 2015;162(3):648-661.
44. Brandt N, Fester L, Rune GM. Neural sex steroids and hippocampal synaptic plasticity. Vitam Horm. 2020;114:125-143.
45. De Roo M, Klauser P, Muller D. LTP promotes a selective long-term stabilization and clustering of dendritic spines. PLoS Biol. 2008;6(9):e219.
46. Zhou L, Fester L, von Blittersdorff B, et al. Aromatase inhibitors induce spine synapse loss in the hippocampus of ovariectomized mice. Endocrinology. 2010;151:1153-1160.
47. Ramakers GJ, Wolfer D, Rosenberger G, et al. Dysregulation of rho GTPases in the alphaPix/Arhgef6 mouse model of X-linked intellectual disability is paralleled by impaired structural and synaptic plasticity and cognitive deficits. Hum Mol Genet. 2012;21(2):268-286.
48. Kretz O, Fester L, Wehrenberg U, et al. Hippocampal synapses depend on hippocampal estrogen synthesis. J Neurosci. 2004;24: 5913-5921.
49. Arnoux I, Audinat E. Fractalkine signaling and microglia functions in the developing brain. Neural Plast. 2015;2015:689404.
50. Shinoda Y, Tanaka T, Tominaga-Yoshino K, Ogura A. Persistent synapse loss induced by repetitive LTD in developing rat hippocampal neurons. PloS One. 2010;5:e10390.
51. Mosser CA, Baptista S, Arnoux I, Audinat E. Microglia in CNS development: shaping the brain for the future. Prog Neurobiol. 2017;149150:1-20.
52. Hoogland IC, Houbolt C, van Westerloo DJ, van Gool WA, van de Beek D. Systemic inflammation and microglial activation: systematic review of animal experiments. J Neuroinflammation. 2015;12:114.
53. Schafer DP, Lehrman EK, Kautzman AG, et al. Microglia sculpt postnatal neural circuits in an activity and complement-dependent manner. Neuron. 2012;74(4):691-705.
54. Pchitskaya E, Bezprozvanny I. Dendritic spines shape analysisclassification or Clusterization? Perspective. Front Synaptic Neurosci. 2020;12:31.
55. Lehrman EK, Wilton DK, Litvina EY, et al. CD47 protects synapses from excess microglia-mediated pruning during development. Neuron. 2018;100(1):120-134.e6.
56. Feinberg I. Schizophrenia: caused by a fault in programmed synaptic elimination during adolescence? J Psychiatr Res. 1982;17(4): 319-334.
57. Bastrikova N, Gardner GA, Reece JM, Jeromin A, Dudek SM. Synapse elimination accompanies functional plasticity in hippocampal neurons. Proc Natl Acad Sci U S A. 2008;105(8):3123-3127.
58. Penzes P, Buonanno A, Passafaro M, Sala C, Sweet RA. Developmental vulnerability of synapses and circuits associated with neuropsychiatric disorders. J Neurochem. 2013;126(2):165-182.
59. Kim H. Differential neural activity in the recognition of old versus new events: an activation likelihood estimation meta-analysis. Hum Brain Mapp. 2013;34:814-836.
60. Auerbach BD, Osterweil EK, Bear MF. Mutations causing syndromic autism define an axis of synaptic pathophysiology. Nature. 2011; 480(7375):63-68.
61. Pfeiffer BE, Huber KM. Current advances in local protein synthesis and synaptic plasticity. J Neurosci. 2006;26(27):7147-7150.
62. Tang H, Zhang Q, Yang L, et al. Reprint of "GPR30 mediates estrogen rapid signaling and neuroprotection". Mol Cell Endocrinol. 2014; 389(1–2):92-98.
63. Nikodemova M, Kimyon RS, De I, Small AL, Collier LS, Watters JJ. Microglial numbers attain adult levels after undergoing a rapid decrease in cell number in the third postnatal week. J Neuroimmunol. 2015;278:280-288.
64. Du Y, Brennan FH, Popovich PG, Zhou M. Microglia maintain the normal structure and function of the hippocampal astrocyte network. Glia. 2022;70(7):1359-1379.
65. Jay TR, von Saucken VE, Muñoz B, et al. TREM2 is required for microglial instruction of astrocytic synaptic engulfment in neurodevelopment. Glia. 2019;67(10):1873-1892.
66. Sumitomo A, Tomoda T. Autophagy in neuronal physiology and disease. Curr Opin Pharmacol. 2021;60:133-140.
67. Damulewicz M, Szypulski K, Pyza E. Glia-neurons cross-talk regulated through autophagy. Front Physiol. 2022;13:886273.
68. Guo R, Xu Y, Xiong W, et al. Autophagy-mediated synaptic refinement and auditory neural pruning contribute to ribbon synaptic maturity in the developing cochlea. Front Mol Neurosci. 2022;15: 850035.
69. Boulanger A, Dura JM. Neuron-glia crosstalk in neuronal remodeling and degeneration: neuronal signals inducing glial cell phagocytic transformation in drosophila. Bioessays. 2022;44(5):e2100254.
70. Zapata-Muñoz J, Villarejo-Zori B, Largo-Barrientos P, Boya P. Towards a better understanding of the neuro-developmental role of autophagy in sickness and in health. Cell Stress. 2021;5(7):99-118.
71. Parkhurst CN, Yang G, Ninan I, et al. Microglia promote learningdependent synapse formation through brain-derived neurotrophic factor. Cell. 2013;155(7):1596-1609.
72. Tremblay M, Lowery RL, Majewska AK. Microglial interactions with synapses are modulated by visual experience. PLoS Biol. 2010;8(11): e1000527.

73. Soch A, Sominsky L, Younesi S, et al. The role of microglia in the second and third postnatal weeks of life in rat hippocampal development and memory. Brain Behav Immun. 2020;88:675-687.
74. Toni N, Buchs PA, Nikonenko I, Bron CR, Muller D. LTP promotes formation of multiple spine synapses between a single axon terminal and a dendrite. Nature. 1999;402(6760):421-425.
75. Schwarz JM, Sholar PW, Bilbo SD. Sex differences in microglial colonization of the developing rat brain. J Neurochem. 2012;120(6):948-963.
76. Schwarz JM, Bilbo SD. Sex, glia, and development: interactions in health and disease. Horm Behav. 2012;62(3):243-253.
77. Guneykaya D, Ivanov A, Hernandez DP, et al. Transcriptional and translational differences of microglia from male and female brains. Cell Rep. 2018;24(10):2773-2783.e6.

78. Ruggiero MJ, Boschen KE, Roth TL, Klintsova AY. Sex differences in early postnatal microglial colonization of the developing rat hippocampus

83. Bolton JL, Short AK, Simeone KA, Daglian J, Baram TZ. Programming of stress-sensitive neurons and circuits by early-life experiences. Front Behav Neurosci. 2019;13:30.
84. Gomez CD, Read J, Acharjee S, Pittman QJ. Early life inflammation increases CA1 pyramidal neuron excitability in a sex and age dependent manner through a chloride homeostasis disruption. J Neurosci. 2019;39(37):7244-7259.

How to cite thisPrengel TM, Brunne B, Rune GM. Sexually differentiated microglia hippocampal synaptic [illegible]: 35(5):e13276.10.11/jne.13276

following a single-day alcohol exposure. J Neuroimmune Pharmacol. 2018;13(2):189-203.
79. Han J, Fan Y, Zhou K, Blomgren K, Harris RA. Uncovering sex differences of rodent microglia. J Neuroinflammation. 2021;18(1):74.
80. Crain JM, Nikodemova M, Watters JJ. Microglia express distinct M1 and M2 phenotypic markers in the postnatal and adult central nervous system in male and female mice. J Neurosci Res. 2013;91(9):
1143-1151.
81. Konkle ATM, McCarthy MM. Developmental time course of estradiol, testosterone, and dihydrotestosterone levels in discrete regions of male and female rat brain. Endocrinology. 2011;152:
223-235.
82. Hammond TR, Dufort C, Dissing-Olesen L, et al. Single-cell RNA sequencing of microglia throughout the mouse lifespan and in the injured brain reveals complex cell-state changes. Immunity. 2019; 50(1):253-271.e6.

Darstellung der Publikation und weiterführende Einordnung

Die vorliegende Dissertation beruht auf der Publikation „Sexually differentiated microglia and CA1 hippocampal synaptic connectivity“, die am 17. April 2023 im Journal of Neuroendocrinology veröffentlicht wurde (Prengel et al., 2023). Die Verweise im Ergebnisteil beziehen sich auf die Abbildungen (Figures) der Veröffentlichung.

Einleitung

Das Gehirn besteht aus 10^{11} Zellen (Gulati, 2015), die untereinander durch Synapsen verbunden sind. Diese speziellen Zellverbindungen übertragen durch chemische Signale das elektrische Membranpotential eines Neurons auf ein nachgeschaltetes weiteres Neuron (Kahle, 2005: 24). Diese Synapsen bestehen aus einer präsynaptischen Verdickung des vorgeschalteten Axons, dem axonalen Bouton und einem postsynaptischen Spine, einer dünnen Ausstülpung der Zellmembran (Harris und Weinberg, 2012). Dazwischen liegt ein Spalt, der als chemische Übertragungsstelle von weitergeleiteten Aktionspotentialen des präsynaptischen Axons durch die Ausschüttung von intrazellulär in Vesikeln gespeicherten Neurotransmittern dient. An der postsynaptischen Membran exzitatorischer Synapsen befindet sich eine elektronendichte Verdickung, die postsynaptische Dichtplatte, in der unter anderem Rezeptoren zur Aufnahme der ausgeschütteten Neurotransmitter liegen (Harris und Weinberg, 2012). Gemäß der Hebb’schen Regel ist die Signalübertragung einer Synapse nur dann erfolgreich, wenn einem präsynaptischen Aktionspotential eine postsynaptische Depolarisation folgt. Erfolgt die Depolarisation vor dem vorgeschalteten Aktionspotential, ist die Synapse schwach bzw. obsolet (Bliss und Lomo, 1973).

Die Verbindung der Nervenzellen ist die Grundlage der Netzwerkbildung im Gehirn. Ein Beispiel hierfür ist die Netzwerkbildung des Hippocampus, der als sogenanntes heteroassoziatives Netzwerk (Lisman und Otmakhova, 2001) unter anderem dem Abgleich sensorischer Informationen aus dem Cortex mit gespeicherten Erinnerungen dient (Bartsch und Wulff, 2015). In der Region Cornu Ammonis 3 (CA3) und dem Gyrus Dentatus (DG) des Hippocampus werden durch reziproke Verschaltungen Erinnerungen des episodischen Gedächtnisses über den Tractus perforans aus dem Cortex abgerufen (Lisman, 1999), in der Region Cornu Ammonis 1 (CA1) mit neuem Input abgeglichen und gegebenenfalls angepasst an den Cortex zurückgeleitet (Bartsch und Wulff, 2015, Lisman und Otmakhova, 2001). Die Verbindung der Region CA3 und CA1 wird durch die Schaffer-Kollateralen, lange Axone aus der Region CA3, die auf postsynaptische Dendriten der Pyramidenzellen im Stratum radiatum der Region CA1 projizieren, gewährleistet (Bartsch und Wulff, 2015). Thema dieser Arbeit ist die Untersuchung der postnatalen Alteration dieser Synapsen.

Gliazellen: Mikroglia und Astrozyten

Mikroglia und Astrozyten sind essenziell für synaptische Übertragung und interagieren mit Neuronen (Lee et al., 2021, Schafer et al., 2013).
Astrozyten sind an der Entwicklung und Ausdifferenzierung von Synapsen durch die Sekretion von Neurotransmittern beteiligt (Papouin et al., 2017) und dem Großteil (50-90%) der Synapsen des Hippocampus angelagert (Farhy-Tselnicker und Allen, 2018).
Mikroglia sind die gehirneigenen Immunzellen. Diese Makrophagen wandern während der embryonalen Entwicklung ins zentrale Nervensystem ein und nehmen dort immunologische Aufgaben wahr (Ginhoux et al., 2010, Johann und Beyer, 2013, Wake et al., 2009). Sie sind aber auch an der postnatalen Gehirnentwicklung beteiligt (Bessis et al., 2007). Verzweigte Mikroglia kontaktieren im adulten Gehirn regelmäßig Synapsen mit ihren Fortsätzen (Wake et al., 2009).

Synaptisches Pruning

Der Begriff synaptisches Pruning (engl. Beschneiden) wurde 1982 von dem Psychiater Irwin Feinberg eingeführt. Feinberg hatte in Post-Mortem-Analysen eine höhere Anzahl von Synapsen im Cortex Neugeborener und Kinder als im Gewebe älterer Menschen beobachtet und folgerte, dass diese Synapsen durch einen unbekannten Prozess verloren gegangen sein mussten (Feinberg, 1982).
Synaptisches Pruning wird seitdem als Verfeinerung und Konsolidierung erfolgreicher synaptischer Verbindung durch die Entfernung von im Sinne der Hebb'schen Regel schwacher Synapsen verstanden (Faust et al., 2021, Horling et al., 2015, Paolicelli et al., 2011, Schafer et al., 2012). Ein Ausbleiben oder eine Verzögerung des synaptischen Prunings wird mit verschiedenen neurologischen Entwicklungsstörungen wie frühkindlichem Autismus (Tian et al., 2024) oder Phenylkentonurie (Horling et al., 2015) assoziiert.
2011 wies die Arbeitsgruppe von Rosa Paolicelli erstmals das Vorhandensein postsynaptischer Spines in Mikroglia nach und zeigte in einem Knock-Out-Modell, in dem die Einwanderung von Mikroglia in den Hippocampus gehemmt wurde, dass die Abwesenheit von Mikroglia zu einer erhöhten Anzahl postsynaptischer Spines führte (Paolicelli et al., 2011).

Mechanismen des synaptischen Prunings

Da Mikroglia als Makrophagen in der Lage sind, Erreger oder Zelldetritus zu phagozytieren (Li und Barres, 2018), untersuchten nachfolgende Studien die immunologischen Signalwege, mit denen Mikroglia aktivitätsabhängig Synapsen erkennen und aufnehmen (Schafer et al., 2012). Es konnte gezeigt werden, dass Mikroglia durch das klassische Komplementsystem schwache Synapsen erkennen sowie präsynaptische Elemente phagozytieren und intrazellulär abbauen (Schafer et al., 2012). Im Hippocampus von 18-20 Tagen alten Mäusen konnte festgestellt werden, dass Mikroglia in einem triggering receptor expressed on myeloid cells 2 (TREM2)-Knock-Out-Modell nicht in der Lage waren postsynaptische Spines zu phagozytieren (Filipello et al., 2018).
Entgegen der ursprünglichen Annahme von Paolicelli, dass Mikroglia postsynaptische Spines phagozytieren (Paolicelli et al., 2011), zeigte die Arbeitsgruppe von Cornelius Gross, die mit hochauflösenden Methoden Mikroglia-Neuron Interaktionen auf ultrastruktureller Ebene untersuchten, dass Mikroglia nur geringfügig neuronales Material von präsynaptischen Boutons aufnehmen und postsynaptische Spines nicht

phagozytieren, sondern von Spine-Köpfen ausgehende dünnste neuronale Fortsätze, die sogenannten Filopodia, von ihrem vorgeschalteten Axon lösten und mit einem anderen Axon neu verknüpfen (Weinhard et al., 2018a).
Filopodia sind feine Vorläufer dendritischer Spines und können sich bei Kontakt mit einem präsynaptischen Axon zu einem Spine verdicken. Im weiteren Verlauf sind viele Spines nur transient, aber stabile Spines maturieren und bilden eine Synapse aus (Holtmaat und Svoboda, 2009).
Die genaueren Mechanismen synaptischer Elimination durch Mikroglia verbleiben somit vorerst ungeklärt (Qin et al., 2022) allerdings werden erfolgreiche Synapsen durch den Rezeptor CD47 vor synaptischem Pruning bewahrt (Lehrman et al., 2018). Dieses Protein schützt körpereigene Strukturen vor Selbsterkennung durch Makrophagen (Elward und Gasque, 2003) und ligiert auf Mikroglia mit Signal Regulatory Protein Alpha (SIRPα) (Lehrman et al., 2018).

Synaptisches Pruning durch Astrozyten und Neuronen

Vereinzelt ist synaptisches Pruning durch Astrozyten ebenfalls beschrieben (Lee et al., 2021), und Neuronen betreiben synaptisches Pruning durch Autophagie (Sumitomo und Tomoda, 2021) und die Verhinderung von neuronaler Autophagie führte zu einer Erhöhung der Spine-Dichte im Temporallappen (Tang et al., 2014, Zapata-Munoz et al., 2021).

Geschlechtsspezifisches Synaptisches Pruning im Hippocampus

Mikrogliazellen sind in ihrem immunologischen Signaling und ihrer phagoyztischen Kapazität sexuell differenziert und unterliegen der Wirkung von Östradiol (Hanamsagar et al., 2017, Nelson et al., 2017, Schwarz et al., 2012) und in der Area preoptica wurde bereits gezeigt, dass sexuell differenzierte Mikroglia zur Maskulinisierung dieser Region beitragen (Lenz et al., 2013). Im Hippocampus weiblicher Mäuse wurde ebenfalls eine gesteigerte mikrogliale Reaktivität und Synapsendichte mit Immunfluoreszenz innerhalb der ersten beiden Lebenswochen gezeigt (Weinhard et al., 2018b), allerdings nicht auf ultrastruktureller Ebene. Da konventionelle Fluoreszenzmikroskope nicht in der Lage sind Synapsen darzustellen, soll in dieser Arbeit die geschlechtsspezifische postnatale Synapsendichte und Neuron-Mikroglia-Interaktionen im Hippocampus elektronenmikroskopisch untersucht und die Auswirkung sexuell differenzierter Mikroglia auf postnatales synaptisches Pruning und Synaptogenese gezeigt werden.

Methoden

Tiere

Für die elektronenmikroskopische Untersuchung wurden jeweils vier weibliche und vier männliche C57BL/6J Mäuse im Alter von zwei, drei und 12 Wochen sowie jeweils drei weibliche und drei männliche Mäuse der gleichen Linie im Alter von vier und acht Wochen verwendet.
Für die Immunfluoreszenzmikroskopie wurden insgesamt 18 heterozygote Thy1eGFP Mäuse (jeweils drei männliche und drei weibliche im Alter von sieben, 14 und 21 Tagen) verwendet.
Für die In-Situ-Hybridisierung und den Western-Blot wurden jeweils drei Männchen und drei Weibchen aus der C57BL/6J-Linie im Alter von zwei Wochen verwendet.
Die Mäuse wurden unter Standardbedingungen untergebracht und mit Futter und Wasser ad libitum versorgt. Die Experimente wurden in Übereinstimmung mit der deutschen Tierschutz-Versuchstierverordnung und der EU-Richtlinie 2010/63/EU zum Schutz der für wissenschaftliche Zwecke verwendeten Tiere durchgeführt. Die Tiere wurden mit Kohlendioxid geopfert, transkardial perfundiert und die Gehirne den unterschiedlichen Experimenten entsprechend aufbereitet und eingebettet.

Zur Erhebung der postnatalen synaptischen Dynamik wurde eine stereologische Bestimmung der Synapsenanzahl in der ersten Schicht des Cornu Ammonis (CA1) des Hippocampus auf elektronenmikroskopischer Ebene bestimmt. Die Hippocampi wurden hierzu mit einer Alkoholreihe entwässert, in Epon 820 (Serva) eingebettet und mit einem Reichert-Jung OmU3 Ultramikrotom in Ultradünnschnitte geschnitten.
Hierbei wurde jeweils in einem 8x8 Mikrometer (μm) großem Ausschnitt bei 2600facher Vergrößerung (CM100 Elektronenmikroskop, Phillips) die Anzahl der Synapsen von einem verblindeten Untersucher ausgewertet. Um Anschnittartefakte zu vermeiden, wurden nur die Synapsen gezählt, an denen jeweils eine prä- und postsynaptische Membran, einen sichtbaren synaptischen Spalt sowie eine postsynaptische Verdickung identifiziert werden konnte. Um die Bestimmung der Anzahl der Synapsen im Volumen des Gewebes zu ermöglichen, wurde dann auf einem im Abstand von 100 Nanometern aufgenommenem Konsekutivschnitt die gleiche Untersuchung durchgeführt. Doppelte Synapsen wurden nicht gezählt. Dieses wurde in jeweils 15 aufeinanderfolgenden Volumina des Hippocampus pro Tier durchgeführt und der Mittelwert errechnet (Leranth et al., 2000, Sterio, 1984).

Fluoreszenzmikroskopie

Für die Fluoreszenzaufnahmen wurden nach der Euthanasie die Gehirne der Tiere in Agarose eingebettet und mit einem Leica-Vibratom 50 μm dicke Gewebeschnitte hergestellt. Diese wurden in zwei Stufen mit folgenden Antikörpern gefärbt:

Primärantikörper und Zielstruktur	Hersteller, Wirt und Konzentration
P2Y Purinerger Rezeptor 12 (P2Y12, Mikroglia-Zellmembran)	AnaSpec 55043A, Kaninchen, 1:500
ionisiertes Calcium-bindendes Adaptermolekül 1 (Iba1, Mikroglia-Zellmembran)	Synaptic Systems 234004, Meerschweinchen, 1:600
Cluster Of Differentiation 68 (CD68, Mikroglia-Lysosom)	Bio-Rad MC1957, Ratte, 1:100

Brain Lipid Binding Protein (BLBP, Astrozyten-Zellembran)	Merck-Millipore ABN14, Kaninchen, 1:500
Saures Gliafaserprotein (GFAP-Astrozyten-Zytoskelett)	Dako Z033401-2, Kaninchen, 1:1000
Grün fluoreszierndes Protein GFP (Neuronen)	Alexa 488, Thermofisher A21311, 1:1000
Sekundärantikörper	
Anti-Meerschweinchen	AF647 Invitrogen A21450, 1:500
Anti-Kaninchen	AF568, Abcam Ab175470, 1:500
Anti-Kaninchen	AF647, Thermofischer A21245, 1:500
Anti-Ratte	AF647, Thermofisher A21247, 1:500
Zellkernfärbung	4′, 6-Diamidin-2-Phenylindol (DAPI) Sigma-Aldrich, 1:5000

Im Anschluss wurden jeweils fünf Schnitte auf einem Objektträger fixiert.

Zur Auswertung wurde mit einem Zeiss-AxioObserver mit integriertem Apotome 2 mit einem Plan-APO 40×/1.4/Öl-Objektiv Z-Stapel von mindestens 40x0,27μm gewonnen. Diese Daten wurden dann mit Oxford Instruments Imaris (version 9.6.0) von einem verblindeten Untersucher ausgewertet. Pro Tier wurde jeweils drei Dendriten erster Ordnung in weniger als 70μm Abstand zum Soma ihrer Ursprungszelle dreidimensional mit einer jeweils individuellen Kontrastschwelle rekonstruiert. Die durchschnittliche Länge der untersuchten Dendriten betrug 64μm.

Die Analyse der Spines wurde mit der Imaris Classify Spines Xtension durchgeführt. Spines wurden in folgende Kategorien eingeteilt: Stubby Spines (Länge <1 μm), Mushroom Spines (maximale Länge >3 μm und maximale Kopfbreite mindestens zweimal größer als die mittlere Halsbreite), long thin Spines (Kopfbreite gleich Halsbreite) und Filopodien (alle Spines, die nicht als eine der oben genannten Kategorien eingestuft wurden und deren Kopfbreite ≤ Halsbreite ist). Die axonale Boutondichte wurde durch Messung der Signalintensität der einzelnen Axonschäfte bestimmt, die über alle Datensätze hinweg normalisiert wurde. Boutons wurden mit dem Spot-Detection-Tool von Imaris mit individuellem Schwellenwert erkannt und als positiv gewertet, wenn die Signalintensität des Boutons die Signalintensität des Axonschafts um 40 % überstieg.

RNA-In-situ-Hybridisierung

Die RNA-In-situ-Hybridisierung wurde mit der RNAscope-Technique40 unter Verwendung des RNAscope-Kits (ACD biotechne) durchgeführt. Eine für P2Y12 mRNA spezifische Zielsonde (ACD biotechne 317601-C2) wurde in Kryoschnitten von jeweils drei weiblichen und drei männlichen Tieren im Alter von zwei Wochen verwendet. Nach dem Hybridisierungsprozess wurden Bilder des linken und rechten Hippocampus mit einem 25×/Luft-Objektiv aufgenommen und in Imaris zusammengefügt. Anschließend wurden rechteckige Flächen mit einer durchschnittlichen Größe von 75480 μm2 aus dem CA1-Feld auf Anlagerung von P2Y12-RNA in Kolokalisation mit DAPI untersucht, um Mikroglia-Zellkerne zu quantifizieren.

Western-Blot

Wildtyp-Wurfgeschwister der Thy1-eGFP-Tiere wurden für die Proteinanalyse mittels Western Blot verwendet. Die Hippocampi wurden aus dem Gehirn entnommen und in flüssigem Stickstoff eingefroren. Nach dem Auftauen bei 4°C wurden die Hippocampi manuell in Radioimmunpräzipitationspuffer (RIPA) und einer Mischung aus Proteinase- (Roche cOmplete Tabletten 1:25) und Phosphataseinhibitoren (Roche PhosSTOP 1:10) homogenisiert. Die Proben wurden bei 13.000 Umdrehungen/Minute für 20 Minuten bei 4°C zentrifugiert, und der Überstand wurde bis zur weiteren Verwendung eingefroren. Anschließend wurden 10 µg jeder Probe auf Nitrocellulosemembranen geblottet. Die unspezifische Bindung von Antikörpern wurde durch Behandlung der Membran mit 5% fettfreier Milchpulverlösung verhindert. Die Inkubation mit dem primären Antikörper erfolgte 12 Stunden lang bei 4 °C in Blocking-Lösung mit dem CD47-Antikörper von RD Systems (Ziege, 1:1000), und als interner Standard wurde Glyceraldehyd-3-Phosphat-Dehydrogenase (GAPDH) verwendet (Life Technology, Maus, 1:200). Für die Sekundärfärbung wurden HRP-konjugierte Maus-Anti-Ziege (Thermofisher, 1:200) und Ziege-Anti-Maus (Thermofisher, 1:200) Antikörper verwendet.

Statistik

Die statistische Analyse wurde mit SPSS 27 für Windows durchgeführt. Jeder Datensatz wurde mit dem Shapiro-Wilk-Test auf Normalverteilung geprüft, und die Datensätze für die ANOVA wurden mit dem Levene-Test auf Homogenität der Varianz geprüft. Die Residuen des für das Regressionsmodell verwendeten Datensatzes wurden auf Normalverteilung und Homoskedastizität untersucht. Für das Regressionsmodell und Chi-Quadrat-Tests wurden Post-hoc-Power-Analysen mit G*Power durchgeführt.
Als Signifikanzniveau wurde ein p-Wert von 5% festgelegt und zur Transparenz die jeweiligen Effektgrößen berichtet. Die gesamte Analyse wurde mit der Benjamini-Hochberg-Prozedur für multiples Testen (Q=0,1) korrigiert.

Ergebnisse

Elektronenmikroskopische Untersuchung der Synapsendichte: Figure 1

Für die gewonnen Daten wurde ein passendes Modell mit einer polynomialen Regressionsanalyse für die Variablen Alter, Alter^2 und Geschlecht erstellt. Hierbei zeigten sich signifikante Ergebnisse für die verknüpften Koeffizienten Alter und Alter^2 aber nicht für den Koeffizienten Geschlecht, sodass die synaptische Dichte vom Alter der Tiere abhängig ist aber nicht vom Geschlecht.
Insgesamt zeigte sich ein Verlauf mit steilem Anstieg des errechneten Modells bis zur vierten Woche und anschließendem geringem Nettoverlust von Synapsen bis zum Ende der Untersuchung, was ein begrenztes synaptisches Pruning nach der vierten Woche nahelegt (**Figure 1C**: n=36; $F(3) = 9.651$; korrigiertes $R^2 = 0,475$; $p = 0,0001$; SC Age = 3,971; $p = 0,0001$; SC Age = −3,822; $p = 0,0001$; power: 0,996)
Um die Ergebnisse von Weinhard und Paolicelli (Paolicelli et al., 2011, Weinhard et al., 2018b) in Kontext zu setzen wurde dann eine Subgruppenanalyse am postnatalen Tag 14 (P14) mit Students T-Test durchgeführt. Hier zeigte sich konkordant zu den Ergebnissen von Weinhard (Weinhard et al., 2018b) eine höhere Synapsenanzahl bei den weiblichen Tieren (**Figure 1D**: n=4; $t = 3,153$; df = 6; mean difference = 2,38; 95% CI (0,83; 3,6); $p = 0,02$; Cohen's $d = 2,229$)

Bestimmung der Mikroglia-Morphologie mit Immunfluoreszenz: Figure 2

Zur Untersuchung der Reaktivität der Mikroglia wurden in einem weiteren Experiment CD68-positive Granula in Mikroglia angefärbt und ihr Volumen dreidimensional rekonstruiert, sowie durch dreidimensionale Rekonstruktion des Oberflächen-Volumen-Verhältnis die Morphologie der Mikroglia bestimmt. Da Mikroglia abhängig von ihrer Reaktivität (Paolicelli et al., 2022) ihre Zellfortsätze einziehen und sich das Zell-Soma verdickt (Schwarz et al., 2012), ist das Oberflächen-Volumen-Verhältnis eine einfache Methode die Reaktivität der Mikroglia in einem Gewebeabschnitt darzustellen.
Hier zeigte sich in beiden Geschlechtern eine Abnahme der Reaktivität der Mikroglia von der ersten bis zur dritten Woche mit einer Verzögerung dieser in weiblichen Mikroglia in der zweiten Woche (**Figure 2D**: n=6, $F = 4,99$; $p = 0,002$; $\eta^2 = 0,49$; P7–P21 mean difference= −0.57; 95% CI (−1,0; −0,14); SE = 0,17; $p = 0,008$; P14 female–male mean difference = −0,93; 95% CI (−1,8; −0,05); SE = 0,27; $p = 0,03$).

Zu diesem Zeitpunkt war das Volumen CD68-positiver Granula, ein Reaktivitätsmarker in weiblichen Mikroglia ebenfalls erhöht (**Figure 2E**: n=3 $F = 23,6$; $\eta^2 = 0,115$; mean difference 152,98; SE = 31,495; 95% CI (65,53; 240,42); $p = 0,008$).

Mikroglia Quantifizierung mit RNA-Scope: Figure 3

Um auszuschließen, dass die Quantifizierung von Mikroglia-Spine-Interaktionen durch unterschiedliche Anzahlen von Mikroglia im weiblichen und männlichen Hippocampus verfälscht wurden, wurde eine Ribonuklein-in-Situ-Fluoreszenz-Hybrydisierung mit einem kommerziellen RNA-Scope Kit durchgeführt. Hierbei wurde P2Y12-RNA, die exklusiv in Mikroglia vorliegt, mit einer Anfärbung der Zellkerne überlappt, um die Kerne mikroglialer Zellen zweifelsfrei zu identifizieren. Dabei zeigten sich keine

Unterschiede in der Anzahl hippocampaler Mikroglia zwischen Männchen und Weibchen (**Figure 3D**: n=6 $t = 0{,}053$; df = 10; mean difference = 0,066; 95% CI (−2,7; 2,83); SE = 1,24; $p = 0{,}96$).

Bestimmung von Mikroglia-Spine-Interaktionen: Figure 4

Um die Interaktion von Mikroglia und Neuronen zu untersuchen, wurde in einem zweiten Experiment die Überlagerung von Mikroglia und postsynaptischer Spines Thy1-Green-flurescent-protein postiver Neuronen mit Immunofluoreszenz dreidimensional rekonstruiert.
Da in bisherigen Arbeiten Mikroglia-Pruning vor allem um die zweite postnatale Woche beschrieben ist (Paolicelli et al., 2011, Weinhard et al., 2018b) wurden die Zeitpunkte postnataler Tag 14 und postnataler Tag 21 (P21) untersucht. Durch die Aufnahme von Z-Stapeln wurde jeweils ein Dendritenabschnitt mit einer durchschnittlichen Länge von 64μm dreidimensional rekonstruiert und die Signalintensität des spezifischen Mikrogliaantikörpers P2Y12 in den Spineköpfen gemessen. Als Cut-Off-Wert wurde eine Intensität von 100 gewählt.
Hier zeigte sich eine im Vergleich über die gesamte Stichprobe häufigere Interaktion der Mikroglia mit Spineköpfen in den weiblichen Tieren an P14 sowie eine verringerte Interaktion in den männlichen Tieren zum gleichen Zeitpunkt (**Figure 4D**: n=2234; $\chi^2(3) = 29{,}06$; $p = 0{,}0001$; Cramer's V = 0,114; power: 0,997; P14 female: $p = 0{,}0001$; Cramer's $V = 00{,}1$; P14 male: $p = 0{,}0003$; Cramer's $V = 0{,}09$).

Bestimmung von Astrozyten-Spine-Interaktionen: Figure 4

Nach der oben aufgeführten Methode wurde ebenfalls die Überlagerung von Astrozyten-Signal und Spineköpfen gemessen. Aufgrund der schlechteren Anfärbbarkeit der Astrozyten mit BLBP wurde ein sensitiverer Cut-Off-Wert mit 50 gewählt. Hier zeigten sich geringradige Unterschiede in der Interaktionshäufigkeit in an P21 (**Figure 4F**: n=1682; $\chi^2(3) = 10{,}481$; $p = 0{,}015$; Cramer's $V = 0{,}08$; power: 0,79).

Spine-Quantifizierung und Typisierung: Figure 5

Weiterhin wurden die Anzahl und Typen postsynaptischer Spines und die Anzahl präsynaptischer Boutons pro 10μm Dendriten- bzw. Axonlänge in Männchen und Weibchen im Alter von zwei und drei Wochen ausgewertet und die Spines nach Typ kategorisiert. Hier zeigte sich ein Überschuss axonaler Boutons in den Weibchen an P14 (**Figure 5A**: n=18; P14: t = 2179; df = 33; mean difference = 5,6; 95% CI (0,37; 10,84); SE = 2,57; $p = 0{,}03$) und keine Unterschiede in der Spinedichte (**Figure 5B**: n=9, P14: $t = -0{,}44$; df = 16; mean difference = −0,63; 95% CI (−3,67; 2,41); SE = 1,55; $p = 0{,}66$; P21: t = −1,04; df = 16; mean difference = −1,49; 95% CI (−4,53; 1,55); SE = 1,55; $p = 0{,}31$).

Western Blot CD47: Figure 6

In einer letzten Untersuchung wurde ein Western-Blot für das Protein CD47 durchgeführt. Dieser Marker schützt Synapsen vor Phagozytose durch Mikroglia (Lehrman et al., 2018) hier konnte kein Unterschied gezeigt werden (n=3, $t = -1292$; df = 4; mean difference = −0,11; 95% CI (−0,34; 0.12); SE = 0,08; $p = 0{,}26$).

Diskussion

Die elektronenmikroskopische Untersuchung der Synapsendichte zeigte keine geschlechtsspezifischen Unterschiede in der postnatalen Reifung des Hippocampus. In beiden Geschlechtern wurde die lineare Steigung der Synapsendichte nach der vierten Woche von einem langsamen Synapsenverlust übertroffen.
Da die Mikroglia-Aktivität sich bereits drei Wochen nach der Geburt deutlich verringert ist und die Anzahl der Mikroglia im Hippocampus nach der dritten Woche abnimmt (Nikodemova et al., 2015) ist der Verlust der Synapsen möglicherweise nicht auf die mikrogliale Aktivität zurückzuführen, sondern auf andere Mechanismen, zum Beispiel durch Astrozytisches Pruning oder neuronale Autophagie.
Nur in der zweiten Woche konnte isoliert im weiblichen Hippocampus eine erhöhte Anzahl Synapsen korrelierend mit einer erhöhten Mikrogliareaktivität und einer höheren Häufigkeit von Mikroglia-Spine-Kontakten festgestellt werden. Ein analoger Anstieg der Spine-Dichte konnte nicht gezeigt werden. Die Anzahl synaptischer Boutons war zum Zeitpunkt P14 im weiblichen Hippocampus ebenfalls erhöht.
Diese Ergebnisse lassen den Rückschluss zu, dass zu diesem Zeitpunkt im weiblichen Hippocampus eine verstärkte Synaptogenese durch sexuell differenzierte Mikroglia induziert wird und parallel zur Bildung neuer Synapsen, wie von Weinhard gezeigt, reaktive Mikroglia die Elimination präsynaptischer Anteile betreiben (Weinhard et al., 2018a).

Sexuelle Differenzierung der Mikroglia und Auswirkung auf Gehirnentwicklung

Die sexuelle Differenzierung der Mikroglia ist vielfältig beschrieben (Hanamsagar et al., 2017, Nelson et al., 2017, Schwarz et al., 2012, Villa et al., 2019). Männliche Mikroglia maturieren früher und ihr Transkriptionsprofil ist proinflammatorischer als das weiblicher Mikroglia (Hanamsagar et al., 2017, Villa et al., 2019, Villa et al., 2018) Weibliche Mikroglia haben stärker ausgeprägte neuroprotektive Eigenschaften und behalten diese selbst nach Transplantation in mikrogliadepletierte männliche Gehirne bei (Villa et al., 2018) und weisen im Hippocampus eine stärkere Phagozytoseaktivität, die sich durch die Wirkung von Östrogen zurückbildet (Nelson et al., 2017). Ursächlich hierfür ist möglicherweise die Testosteronwoge während des Deszensus Testis und der Einfluss des daraus resultierenden perinatal erhöhten Östrogenspiegel im männlichen Gehirn (Lenz et al., 2013, Nelson et al., 2017, Rhoda et al., 1984).

Bidirektionale Rolle der Mikroglia in Synaptogenese und synaptischem Pruning und Wirkung von Östrogen

Die vorliegenden Ergebnisse zeigen eine Korrelation des steilen Anstiegs der Synapsen zwischen der zweiten und vierten Lebenswoche und der gesteigerten mikroglialen Reaktivität. In vorhergehenden Arbeiten wurde bereits gezeigt, dass Mikroglia nicht nur an der Entfernung von synaptischem Material in unterschiedlichen Arealen des Gehirns beteiligt sind (Filipello et al., 2018, Pöpplau et al., 2024, Schafer et al., 2012, Schafer et al., 2013, Schwarz et al., 2012, Soch et al., 2020, Weinhard et al., 2018a) und ebenso an der Induktion der Ausbildung neuer Spines und Filopodia durch die Ausschüttung von Brain Derived Neurotrophic Factor (BDNF) (Parkhurst et al., 2013) und Interleukin-10 in Abhängigkeit von Östrogen (Miyamoto et al., 2016).
Östrogen unterdrückt in Mikroglia die Aktivierung des reaktiven Interleukin 1ß-sezernierenden Zustandes (Thakkar et al., 2016) und lässt bereits reaktive zytotoxische Mikroglia in einen alternativen neuroprotektiven Aktivierungszustand

wechseln, der durch die Ausschüttung von Interleukin 10 gekennzeichnet ist (Habib et al., 2014) und den Ausgangszustand, der von Miyamoto beschriebenen Spine-Induktion darstellt (Miyamoto et al., 2016). Ebenso ist die Induktion von synaptischer Plastizität im Hippocampus durch repetitive Magnetstimulation abhängig von der Freisetzung proinflammatorischer Zytokine durch Mikroglia (Eichler et al., 2023). In einer rezenten Studie wurde zudem nachgewiesen, dass Mikroglia im präfrontalen Cortex entscheidend zur Steigerung der elektrophysiologischen Synchronität beitragen und Mikrogliadepletion vor dem 30. Lebenstag zu langfristigen kognitiven Defiziten führt (Pöpplau et al., 2024).

Synaptogenese und Multispineboutons

Eine Ursache für die Induktion von Synaptogenese ist die von Weinhard beschriebene Umverlagerung von Filopodien an einen bereits existierenden präsynpatischen Bouton (Weinhard et al., 2018a). An diesen Multi-Spine-Boutons (MSB) werden wiederum neue Synapsen gebildet (Toni et al., 1999, Weinhard et al., 2018a). Hierdurch konsolidieren Mikroglia starke synaptische Verbindungen, was die Wahrscheinlichkeit einer erfolgreichen Auslösung eines exzitatorischen postsynaptischen Signals erhöht (Toni et al., 1999).

Schlussfolgerung

Die Ergebnisse dieser Arbeit sind vereinbar mit der Annahme einer gesteigerten Synaptogenese im weiblichen Hippocampus in der zweiten postnatalen Woche und gesteigerte Multi-Spine-Bouton-Formation im Zusammenspiel mit gesteigerter Neuron-Mikroglia Interaktion durch reaktive Mikroglia.
Die Hypothese der Bildung von MSBs konnte mit den genutzten Methoden nicht untersucht werden, sie wird aber durch den fehlenden Anstieg der Anzahl postsynaptischer Spines und axonaler Boutons zwischen P14 und P21 (dem Zeitpunkt der stärksten Synaptogenese) bekräftigt.
Letztendlich aber zeigt diese Arbeit auch, dass die durch Mikroglia induzierte synaptische Reorganisation des Hippocampus keinen langfristigen geschlechtsspezifischen Unterschied zur Folge hat.

Stärken und Schwächen der Arbeit

Die vorliegende Arbeit zeigt den Verlauf der postnatalen synaptischen Dynamik in der CA1-Region des Hippocampus bis zur adulten Phase. Im Gegensatz zu vorhergehenden Untersuchungen über synaptisches Pruning (Filipello et al., 2018, Lehrman et al., 2018, Paolicelli et al., 2011, Weinhard et al., 2018b) wurden Synapsen quantitativ auf ultrastruktureller Ebene untersucht. Nur diese Methode lässt eine zweifellose Identifikation von Synapsen zu, die mit Fluoreszenz- oder konfokaler Mikroskopie oder durch die Bestimmung der Spine-Dichte nicht im gleichen Maße dargestellt werden können (Bastrikova et al., 2008).
.
Die Schwäche der Arbeit liegt darin, dass die Elektronenmikroskopische Untersuchung zwar mit der Mikroglia-Aktivität korreliert, aber im experimentellen Design keine kausale Verbindung zwischen Mikroglia und Synapsenanzahl untersucht wird. So kann der Einfluss der Mikroglia auf die Synaptogenese oder die Möglichkeit von simultan verlaufendem synaptischen Pruning nicht belegt oder ausgeschlossen werden.

Literaturverzeichnis

BARTSCH, T. & WULFF, P. 2015. The hippocampus in aging and disease: From plasticity to vulnerability. *Neuroscience,* 309**,** 1-16.

BASTRIKOVA, N., GARDNER, G. A., REECE, J. M., JEROMIN, A. & DUDEK, S. M. 2008. Synapse elimination accompanies functional plasticity in hippocampal neurons. *Proc Natl Acad Sci U S A,* 105**,** 3123-7.

BESSIS, A., BECHADE, C., BERNARD, D. & ROUMIER, A. 2007. Microglial control of neuronal death and synaptic properties. *Glia,* 55**,** 233-8.

BLISS, T. V. & LOMO, T. 1973. Long-lasting potentiation of synaptic transmission in the dentate area of the anaesthetized rabbit following stimulation of the perforant path. *J Physiol,* 232**,** 331-56.

EICHLER, A., KLEIDONAS, D., TURI, Z., FLIEGAUF, M., KIRSCH, M., PFEIFER, D., MASUDA, T., PRINZ, M., LENZ, M. & VLACHOS, A. 2023. Microglial Cytokines Mediate Plasticity Induced by 10 Hz Repetitive Magnetic Stimulation. *J Neurosci,* 43**,** 3042-3060.

ELWARD, K. & GASQUE, P. 2003. "Eat me" and "don't eat me" signals govern the innate immune response and tissue repair in the CNS: emphasis on the critical role of the complement system. *Mol Immunol,* 40**,** 85-94.

FARHY-TSELNICKER, I. & ALLEN, N. J. 2018. Astrocytes, neurons, synapses: a tripartite view on cortical circuit development. *Neural Dev,* 13**,** 7.

FAUST, T. E., GUNNER, G. & SCHAFER, D. P. 2021. Mechanisms governing activity-dependent synaptic pruning in the developing mammalian CNS. *Nat Rev Neurosci,* 22**,** 657-673.

FEINBERG, I. 1982. Schizophrenia: caused by a fault in programmed synaptic elimination during adolescence? *J Psychiatr Res,* 17**,** 319-34.

FILIPELLO, F., MORINI, R., CORRADINI, I., ZERBI, V., CANZI, A., MICHALSKI, B., ERRENI, M., MARKICEVIC, M., STARVAGGI-CUCUZZA, C., OTERO, K., PICCIO, L., CIGNARELLA, F., PERRUCCI, F., TAMBORINI, M., GENUA, M., RAJENDRAN, L., MENNA, E., VETRANO, S., FAHNESTOCK, M., PAOLICELLI, R. C. & MATTEOLI, M. 2018. The Microglial Innate Immune Receptor TREM2 Is Required for Synapse Elimination and Normal Brain Connectivity. *Immunity,* 48**,** 979-991 e8.

GINHOUX, F., GRETER, M., LEBOEUF, M., NANDI, S., SEE, P., GOKHAN, S., MEHLER, M. F., CONWAY, S. J., NG, L. G., STANLEY, E. R., SAMOKHVALOV, I. M. & MERAD, M. 2010. Fate mapping analysis reveals that adult microglia derive from primitive macrophages. *Science,* 330**,** 841-5.

GULATI, A. 2015. Understanding neurogenesis in the adult human brain. *Indian J Pharmacol,* 47**,** 583-4.

HABIB, P., SLOWIK, A., ZENDEDEL, A., JOHANN, S., DANG, J. & BEYER, C. 2014. Regulation of hypoxia-induced inflammatory responses and M1-M2 phenotype switch of primary rat microglia by sex steroids. *J Mol Neurosci,* 52**,** 277-85.

HANAMSAGAR, R., ALTER, M. D., BLOCK, C. S., SULLIVAN, H., BOLTON, J. L. & BILBO, S. D. 2017. Generation of a microglial developmental index in mice and in humans reveals a sex difference in maturation and immune reactivity. *Glia,* 65**,** 1504-1520.

HARRIS, K. M. & WEINBERG, R. J. 2012. Ultrastructure of synapses in the mammalian brain. *Cold Spring Harb Perspect Biol,* 4.

HOLTMAAT, A. & SVOBODA, K. 2009. Experience-dependent structural synaptic plasticity in the mammalian brain. *Nat Rev Neurosci,* 10**,** 647-58.

HORLING, K., SCHLEGEL, G., SCHULZ, S., VIERK, R., ULLRICH, K., SANTER, R. & RUNE, G. M. 2015. Hippocampal synaptic connectivity in phenylketonuria. *Hum Mol Genet,* 24**,** 1007-18.

JOHANN, S. & BEYER, C. 2013. Neuroprotection by gonadal steroid hormones in acute brain damage requires cooperation with astroglia and microglia. *J Steroid Biochem Mol Biol,* 137**,** 71-81.

KAHLE, W. 2005. *Nervensystem und Sinnesorgane [noch mehr Klinikbezüge]*, Thieme.

LEE, S. H., REZZONICO, M. G., FRIEDMAN, B. A., HUNTLEY, M. H., MEILANDT, W. J., PANDEY, S., CHEN, Y. J., EASTON, A., MODRUSAN, Z., HANSEN, D. V., SHENG, M. & BOHLEN, C. J. 2021. TREM2-independent oligodendrocyte, astrocyte, and T cell responses to tau and amyloid pathology in mouse models of Alzheimer disease. *Cell Rep,* 37**,** 110158.

LEHRMAN, E. K., WILTON, D. K., LITVINA, E. Y., WELSH, C. A., CHANG, S. T., FROUIN, A., WALKER, A. J., HELLER, M. D., UMEMORI, H., CHEN, C. & STEVENS, B. 2018. CD47 Protects Synapses from Excess Microglia-Mediated Pruning during Development. *Neuron,* 100**,** 120-134.e6.

LENZ, K. M., NUGENT, B. M., HALIYUR, R. & MCCARTHY, M. M. 2013. Microglia are essential to masculinization of brain and behavior. *J Neurosci,* 33**,** 2761-72.

LERANTH, C., SHANABROUGH, M. & HORVATH, T. L. 2000. Hormonal regulation of hippocampal spine synapse density involves subcortical mediation. *Neuroscience,* 101**,** 349-56.

LI, Q. & BARRES, B. A. 2018. Microglia and macrophages in brain homeostasis and disease. *Nat Rev Immunol,* 18**,** 225-242.

LISMAN, J. E. 1999. Relating hippocampal circuitry to function: recall of memory sequences by reciprocal dentate-CA3 interactions. *Neuron,* 22**,** 233-42.

LISMAN, J. E. & OTMAKHOVA, N. A. 2001. Storage, recall, and novelty detection of sequences by the hippocampus: elaborating on the SOCRATIC model to account for normal and aberrant effects of dopamine. *Hippocampus,* 11**,** 551-68.

MIYAMOTO, A., WAKE, H., ISHIKAWA, A. W., ETO, K., SHIBATA, K., MURAKOSHI, H., KOIZUMI, S., MOORHOUSE, A. J., YOSHIMURA, Y. & NABEKURA, J. 2016. Microglia contact induces synapse formation in developing somatosensory cortex. *Nat Commun,* 7**,** 12540.

NELSON, L. H., WARDEN, S. & LENZ, K. M. 2017. Sex differences in microglial phagocytosis in the neonatal hippocampus. *Brain Behav Immun,* 64**,** 11-22.

NIKODEMOVA, M., KIMYON, R. S., DE, I., SMALL, A. L., COLLIER, L. S. & WATTERS, J. J. 2015. Microglial numbers attain adult levels after undergoing a rapid decrease in cell number in the third postnatal week. *J Neuroimmunol,* 278**,** 280-8.

PAOLICELLI, R. C., BOLASCO, G., PAGANI, F., MAGGI, L., SCIANNI, M., PANZANELLI, P., GIUSTETTO, M., FERREIRA, T. A., GUIDUCCI, E., DUMAS, L., RAGOZZINO, D. & GROSS, C. T. 2011. Synaptic pruning by microglia is necessary for normal brain development. *Science,* 333**,** 1456-8.

PAOLICELLI, R. C., SIERRA, A., STEVENS, B., TREMBLAY, M. E., AGUZZI, A., AJAMI, B., AMIT, I., AUDINAT, E., BECHMANN, I., BENNETT, M., BENNETT, F., BESSIS, A., BIBER, K., BILBO, S., BLURTON-JONES, M., BODDEKE, E., BRITES, D., BRÔNE, B., BROWN, G. C., BUTOVSKY, O., CARSON, M. J., CASTELLANO, B., COLONNA, M., COWLEY, S. A., CUNNINGHAM, C., DAVALOS, D., DE JAGER, P. L., DE STROOPER, B., DENES, A., EGGEN, B. J. L., EYO, U., GALEA, E., GAREL, S., GINHOUX, F., GLASS, C. K., GOKCE, O., GOMEZ-NICOLA, D., GONZÁLEZ, B., GORDON, S., GRAEBER, M. B., GREENHALGH, A. D., GRESSENS, P., GRETER, M., GUTMANN, D. H., HAASS, C., HENEKA, M. T., HEPPNER, F. L., HONG, S., HUME, D. A., JUNG, S., KETTENMANN, H., KIPNIS, J., KOYAMA, R., LEMKE, G., LYNCH, M., MAJEWSKA, A., MALCANGIO, M., MALM, T., MANCUSO, R., MASUDA, T., MATTEOLI, M., MCCOLL, B. W., MIRON, V. E., MOLOFSKY, A. V., MONJE, M., MRACSKO, E., NADJAR, A., NEHER, J. J., NENISKYTE, U., NEUMANN, H., NODA, M., PENG, B., PERI, F., PERRY, V. H., POPOVICH, P. G., PRIDANS, C., PRILLER, J., PRINZ, M., RAGOZZINO, D., RANSOHOFF, R. M., SALTER, M. W., SCHAEFER, A., SCHAFER, D. P., SCHWARTZ, M., SIMONS, M., SMITH, C. J., STREIT, W. J., TAY, T. L., TSAI, L. H., VERKHRATSKY, A., VON BERNHARDI, R., WAKE, H., WITTAMER, V., WOLF, S. A., WU, L. J. & WYSS-CORAY, T. 2022. Microglia states and nomenclature: A field at its crossroads. *Neuron,* 110**,** 3458-3483.

PAPOUIN, T., DUNPHY, J., TOLMAN, M., FOLEY, J. C. & HAYDON, P. G. 2017. Astrocytic control of synaptic function. *Philos Trans R Soc Lond B Biol Sci,* 372.

PARKHURST, C. N., YANG, G., NINAN, I., SAVAS, J. N., YATES, J. R., 3RD, LAFAILLE, J. J., HEMPSTEAD, B. L., LITTMAN, D. R. & GAN, W. B. 2013. Microglia promote learning-dependent synapse formation through brain-derived neurotrophic factor. *Cell,* 155**,** 1596-609.

PÖPPLAU, J. A., SCHWARZE, T., DOROFEIKOVA, M., POCHINOK, I., GÜNTHER, A., MARQUARDT, A. & HANGANU-OPATZ, I. L. 2024. Reorganization of adolescent prefrontal cortex circuitry is required for mouse cognitive maturation. *Neuron,* 112**,** 421-440.e7.

PRENGEL, T. M., BRUNNE, B., HABIBALLA, M. & RUNE, G. M. 2023. Sexually differentiated microglia and CA1 hippocampal synaptic connectivity. *J Neuroendocrinol,* 35**,** e13276.

QIN, Q., WANG, M., LI, H., XU, Z. D. & TANG, Y. 2022. Editorial: The role of microglia in the pathogenesis of neurodegenerative diseases. *Front Aging Neurosci,* 14**,** 1105896.

RHODA, J., CORBIER, P. & ROFFI, J. 1984. Gonadal steroid concentrations in serum and hypothalamus of the rat at birth: aromatization of testosterone to 17 beta-estradiol. *Endocrinology,* 114**,** 1754-60.

SCHAFER, D. P., LEHRMAN, E. K., KAUTZMAN, A. G., KOYAMA, R., MARDINLY, A. R., YAMASAKI, R., RANSOHOFF, R. M., GREENBERG, M. E., BARRES, B. A. & STEVENS, B. 2012. Microglia sculpt postnatal neural circuits in an activity and complement-dependent manner. *Neuron,* 74**,** 691-705.

SCHAFER, D. P., LEHRMAN, E. K. & STEVENS, B. 2013. The "quad-partite" synapse: microglia-synapse interactions in the developing and mature CNS. *Glia,* 61**,** 24-36.

SCHWARZ, J. M., SHOLAR, P. W. & BILBO, S. D. 2012. Sex differences in microglial colonization of the developing rat brain. *J Neurochem,* 120**,** 948-63.

SOCH, A., SOMINSKY, L., YOUNESI, S., DE LUCA, S. N., GUNASEKARA, M., BOZINOVSKI, S. & SPENCER, S. J. 2020. The role of microglia in the second and third postnatal weeks of life in rat hippocampal development and memory. *Brain Behav Immun,* 88**,** 675-687.

STERIO, D. C. 1984. The unbiased estimation of number and sizes of arbitrary particles using the disector. *J Microsc,* 134**,** 127-36.

SUMITOMO, A. & TOMODA, T. 2021. Autophagy in neuronal physiology and disease. *Curr Opin Pharmacol,* 60**,** 133-140.

TANG, H., ZHANG, Q., YANG, L., DONG, Y., KHAN, M., YANG, F., BRANN, D. W. & WANG, R. 2014. Reprint of "GPR30 mediates estrogen rapid signaling and neuroprotection". *Mol Cell Endocrinol,* 389**,** 92-8.

THAKKAR, R., WANG, R., SAREDDY, G., WANG, J., THIRUVAIYARU, D., VADLAMUDI, R., ZHANG, Q. & BRANN, D. 2016. NLRP3 Inflammasome Activation in the Brain after Global Cerebral Ischemia and Regulation by 17beta-Estradiol. *Oxid Med Cell Longev,* 2016**,** 8309031.

TIAN, Y., XIAO, X., LIU, W., CHENG, S., QIAN, N., WANG, L., LIU, Y., AI, R. & ZHU, X. 2024. TREM2 improves microglia function and synaptic development in autism spectrum disorders by regulating P38 MAPK signaling pathway. *Mol Brain,* 17**,** 12.

TONI, N., BUCHS, P. A., NIKONENKO, I., BRON, C. R. & MULLER, D. 1999. LTP promotes formation of multiple spine synapses between a single axon terminal and a dendrite. *Nature,* 402**,** 421-5.

VILLA, A., DELLA TORRE, S. & MAGGI, A. 2019. Sexual differentiation of microglia. *Front Neuroendocrinol,* 52**,** 156-164.

VILLA, A., GELOSA, P., CASTIGLIONI, L., CIMINO, M., RIZZI, N., PEPE, G., LOLLI, F., MARCELLO, E., SIRONI, L., VEGETO, E. & MAGGI, A. 2018. Sex-Specific Features of Microglia from Adult Mice. *Cell Rep,* 23**,** 3501-3511.

WAKE, H., MOORHOUSE, A. J., JINNO, S., KOHSAKA, S. & NABEKURA, J. 2009. Resting microglia directly monitor the functional state of synapses in vivo and determine the fate of ischemic terminals. *J Neurosci,* 29**,** 3974-80.

WEINHARD, L., DI BARTOLOMEI, G., BOLASCO, G., MACHADO, P., SCHIEBER, N. L., NENISKYTE, U., EXIGA, M., VADISIUTE, A., RAGGIOLI, A., SCHERTEL, A., SCHWAB, Y. & GROSS, C. T. 2018a. Microglia remodel synapses by presynaptic trogocytosis and spine head filopodia induction. *Nat Commun,* 9**,** 1228.

WEINHARD, L., NENISKYTE, U., VADISIUTE, A., DI BARTOLOMEI, G., AYGUN, N., RIVIERE, L., ZONFRILLO, F., DYMECKI, S. & GROSS, C. 2018b. Sexual dimorphism of microglia and synapses during mouse postnatal development. *Dev Neurobiol,* 78**,** 618-626.

ZAPATA-MUNOZ, J., VILLAREJO-ZORI, B., LARGO-BARRIENTOS, P. & BOYA, P. 2021. Towards a better understanding of the neuro-developmental role of autophagy in sickness and in health. *Cell Stress,* 5**,** 99-118.

Zusammenfassung

Mikroglia, die gehirneigenen Immunzellen, sind auch an der postnatalen Entwicklung des Gehirns beteiligt und spielen eine relevante Rolle bei der Synaptogenese und synaptischem Pruning.
Synaptisches Pruning ist ein Prozess der postnatalen Hirnentwicklung, bei dem überzählige Synapsen entfernt werden. Die genauen Mechanismen in diesem Zusammenhang sind aber weithin unverstanden. In dieser Arbeit wurden über den Zeitraum von 12 Wochen nach der Geburt die Dynamik der Synapsendichte in der CA1-Region des weiblichen und männlichen Hippocampus von C57BL/6J Mäusen mit Elektronenmikroskopie verglichen. Hierbei zeigten sich keine geschlechtsabhängigen Unterschiede über den gesamten Verlauf. Nur am vierzehnten Tag nach der Geburt wiesen die weiblichen Tiere eine signifikant höhere Synapsendichte auf. In Korrelation zeigten weibliche Mikroglia zu diesem Zeitpunkt eine reaktivere Morphologie und erhöhte CD68-positive Granula. Die Inklusion postsynaptischer Spines durch Mikroglia-Fortsätze fand zu diesem Zeitpunkt ebenfalls häufiger in weiblichen Tieren als in männlichen statt. Da zwischen zweiter und dritter Woche die Anzahl der Synapsen stark ansteigt, präsynaptische Boutons und postsynaptische Spines aber unverändert sind, ist die Bildung von Multispineboutons, axonale Boutons denen mehrere Spines angelagert sind und die zur Konsolidierung synaptischer Verbindungen beitragen, naheliegend und reaktive Mikroglia könnten bei der Bildung von Multispineboutons eine Rolle spielen. Langfristig resultierten diese Beobachtungen aber nicht in sexuell differenzierter hippocampaler synaptischer Konnektivität.

Summary

Microglia, the brain's own immune cells, are also involved in the postnatal development of the brain and play a relevant role in both synaptogenesis and synaptic pruning.
Synaptic pruning is a process of postnatal brain development in which excess synapses are removed. However, the exact mechanisms in this context are not well understood. In this study, the dynamics of synapse density in the CA1 region of the female and male hippocampus of C57BL/6J mice were compared by electron microscopy over a period of 12 weeks after birth. There were no sex-dependent differences over the entire course of the study. Only on the fourteenth day after birth did the female animals exhibit a significantly higher synapse density. In correlation, female microglia showed a more relative morphology and increased CD68-positive granules at this time point and also inclusion of postsynaptic spines by microglial processes was more frequent in females than in males. Since the number of synapses increased strongly between the second and third week but presynaptic boutons and postsynaptic spines remained unchanged, the formation of multispine boutons, axonal boutons to which several spines are attached and which contribute to the consolidation of synaptic connections, is obvious and reactive microglia could play a role in the formation of multispine boutons. In the long term, however, these observations did not result in sexually differentiated hippocampal synaptic connectivity.

Erklärung des Eigenanteils an der Publikation

Der Eigenanteil an dieser Publikation umfasst an den einzelnen Experimenten jeweils:

Die Auswertung der durch das Institut zur Verfügung gestellten Elektronenmikroskopischen Bilder.

Die Einbettung und Anfertigung der Gewebeschnitte für die Immunfluoreszenz aus bereitgestelltem Gehirngewebe, sowie die Färbung der Schnitte, die Durchführung der Fluoreszenzmikroskopie sowie die Rekonstruktion und Auswertung mit Imaris.

Die Durchführung der RNA-Scope Methode erfolgte unter enger Anleitung von Dr. Bianka Brunne, die Herstellung der Cryo-Schnitte erfolgte durch Helga Herborth.

Die Durchführung des Western-Blots erfolgte unter enger Anleitung von Christiane Schröder.

Die Kuration und statistische Auswertung aller Daten mit SPSS 27 erfolgte in Eigenleistung.

Im Rahmen der Publikation erfolgte die Anfertigung eines Entwurfes. Die Erstellung der finalen Version erfolgte in Zusammenarbeit mit Dr. Bianka Brunne und Prof. Gabriele Rune. Die Abbildungen wurden in Eigenleistung angefertigt mit technischer Unterstützung durch Alina Jahrmarkt.

Danksagung

Danken möchte ich den Personen, die zur Entstehung und dem Abschluss dieser Arbeit beigetragen haben:

Zuallererst meiner Doktormutter Professor Gabriele Rune für die Möglichkeit in ihrem Institut zu promovieren, für die Förderung meines wissenschaftlichen Interesses und für Mentoring mit nachhaltigem Einfluss auf meinen weiteren Werdegang.

Gleichermaßen meinen beiden BetreuerInnen Dr. Bianka Brunne und Dr. Lepu Zhou für die Einarbeitung in die Methoden, die Beantwortung ungezählter Fragen und besonders Dr. Zhou fürs Mutmachen zu Beginn der Doktorandenzeit.

Weiterhin bei allen KollegInnen und technischen AssistentInnen am Institut für Neuroanatomie, besonders Dr. Moataz Habiballa, Herdis Hamann, Christiane Schröder, Janice Graw, Helga Herbort, Barbara Holstermann, Liz Grundy und Verona Schütze.

Außerdem möchte ich mich bei Ute Prengel, Rudi Albrecht und Hildegard Pape bedanken für ihre fortwährende Unterstützung, ohne die ich das Studium und Doktorandenzeit nicht hätte bewältigen können.

Zuletzt aber nicht an letzter Stelle geht mein Dank an Alina Jahrmarkt, nicht nur für professionelle Hilfe beim Layout der Abbildungen, sondern vor allem für Ruhe und Kraft, wenn mir beides gefehlt hat.

Entfällt aus datenschutzrechtlichen Gründen

Eidesstattliche Erklärung

Ich versichere ausdrücklich, dass ich die Arbeit selbständig und ohne fremde Hilfe verfasst, andere als die von mir angegebenen Quellen und Hilfsmittel nicht benutzt und die aus den benutzten Werken wörtlich oder inhaltlich entnommenen Stellen einzeln nach Ausgabe (Auflage und Jahr des Erscheinens), Band und Seite des benutzten Werkes kenntlich gemacht habe.
Ferner versichere ich, dass ich die Dissertation bisher nicht einem Fachvertreter an einer anderen Hochschule zur Überprüfung vorgelegt oder mich anderweitig um Zulassung zur Promotion beworben habe.
Ich erkläre mich einverstanden, dass meine Dissertation vom Dekanat der Medizinischen Fakultät mit einer gängigen Software zur Erkennung von Plagiaten überprüft werden kann.

Unterschrift: .....